AN ABSTRACT OF THE THESIS OF

Danielle P. Jansik for the degree of Master of Science in Chemical Engineering presented on October 2, 2009.

Title: Flow Processes in the Dry Regime: The Effect on Capillary Barrier Performance

Abstract approved:

Dorthe Wildenschild

Engineered capillary barriers typically consist of two layers of granular materials designed so that the contrast in sediment hydrologic properties and sloping interface retains infiltrating water in the upper layer. We report here on the results of two bench-top capillary barrier experiments, and associated modeling. These experiments were conducted to better understand the behavior of capillary barriers in particular with respect to an engineered barrier system proposed at the potential high-level nuclear waste site at Yucca Mountain, Nevada, where different engineered barriers have been under consideration throughout the site development process (Carter and Pigford 2005; Tidwell et al. 2003). We measured hydrologic parameters for both coarse materials using standard methods and found that the two materials had similar hydrologic properties despite being morphologically different (round, uniform vs. angular, non-uniform). The rounded sand provided a better functioning capillary barrier than the angular sand, but neither experiment could be characterized as a

perfectly working capillary barrier. In both cases, more than 93% of the infiltrating water was successfully diverted from the lower layer, but infiltration into the underlying layer was observed in both systems. Our experimental results show that capillary barriers designed based on standard hydrologic property measurements may result in invalid prediction of the system behavior. Moreover, our numerical simulations of these experiments show that the predicted capillary barrier performance was highly sensitive to physically realistic variability in model hydrologic parameter values. Based on this work, we believe that other non-continuum processes such as vapor diffusion and film flow contribute to the observed phenomena and are important aspects to consider with respect to capillary barrier design, as well as dry vadose zone processes in general. By applying a theoretical film flow equation representative of sediment surface geometries we were able to show that infiltration into the underlying sediment layer can be dominated by water film flow, a characteristic that is typically not considered in mainstream numerical models.

Flow Processes in the Dry Regime: The Effect on Capillary Barrier Performance

by

Danielle P. Jansik

A THESIS

submitted to

Oregon State University

in partial fulfillment of

the requirements for the

degree of

Master of Science

Presented October 2, 2009

Commencement June 2010

Master of Science thesis of Danielle P. Jansik presented on October 2, 2009.

APPROVED:

Major Professor, representing Chemical Engineering

Head of the School of Chemical, Biological and Environmental Engineering

Dean of the Graduate School

I understand that my thesis will become part of the permanent collection of Oregon State University Libraries. My signature below authorizes release of my thesis to any reader upon request.

Danielle P. Jansik, Author

ACKNOWLEDGEMENTS

I would like to thank my committee members, Dr. Dorthe Wildenschild, Dr. Brian Wood, and Dr. Maria Dragila for their help and support throughout my degree program. A special thanks to Dr. Dorthe Wildenschild for her encouragement, suggestions, and patience as I slowly find my path through a somewhat sinuous research career. My true appreciation to Dr. Maria Dragila who assisted with my understanding of water film infiltration, to Gaurav Saini who conducted Atomic Force Microscopy measurements, and to my professors, teachers, and advisors through the years.

I am also grateful to the staff and support at Pacific Northwest National Lab, including Dr. Dawn Wellman and Dr. Eric Pierce who motivated me to take the time to complete a master's thesis. Thanks to my mom Jenelle Jansik for the years of love and support and to my partner Graysen Squeochs for his unending love and patience.

CONTRIBUTION OF AUTHORS

Dr. Dorthe Wildenschild completed the initial experiments included in the manuscript, conducted significant amounts of data analysis, writing, and calculations of vapor flux. Dr. Nina Rosenburg completed the experimental modeling. Dorthe Wildenschild provided continuous guidance throughout data collection and analysis, as well as reviews and suggestions in preparation of and during the writing of the manuscript.

TABLE OF CONTENTS

TABLE OF CONTENTS (continued)

LIST OF FIGURES

LIST OF FIGURES (continued)

LIST OF TABLES

DEDICATION

I dedicate this thesis to my mom, Jenelle Patricia Jansik,

who gave me both roots and wings.

Chapter 1: Introduction

Responsible long-term waste storage and disposal is an integral component of minimizing groundwater and surface water contamination. Acid mine drainage (Weeks et al. 2004), landfills (Yanful et al. 2006), spent nuclear waste (Carter and Pigford 2005), and other hazardous materials (Ross 1990) pose considerable risk to groundwater and surface water resources. To minimize risk of contamination, significant resources have been allocated to investigate primary and secondary waste isolation technologies (Carter and Pigford 2005). One such method is the use of natural and artificial capillary barrier systems.

Engineered capillary barriers typically consist of two layers of granular materials designed so that the contrast in sediment hydrologic properties and sloping interface retains infiltrating water in the upper layer and is diverted away from sensitive material. Capillary barrier systems consist of two or more contrasting layers of soil, sand, or gravel in which a fine sediment overlays a coarse-grained material on a sloping interface. Figure 1 is a schematic of a capillary barrier system. As dictated by the Young-Laplace equation, capillary forces in the overlying sediments are significantly stronger, which prevents water from infiltrating into the underlying coarse layer; instead excess water is diverted along the fine-coarse interface down dip (Ross 1990; Oldenburg and Pruess 1993; Webb 1997; Smesrud and Selker 2001; Weeks et al. 2004).

The following literature review (Chapter 2) examines the fundamentals of capillary barrier systems, experimental modeling, and provides a theoretical analysis of vapor

diffusion and water film flow. The attached manuscript (Chapter 3) applies current theory and understanding to two capillary barrier experiments and isolates the controlling flow process in the dry regime.

The underlying motivation for research conducted in this thesis is to provide a low failure tolerance design for diversion of infiltrating fluid in a long term geologic nuclear waste repository. By diverting flow and reducing contact of fluid with encapsulated nuclear wasteforms the over overall risk of radionuclide transport and human exposure is thus reduced.

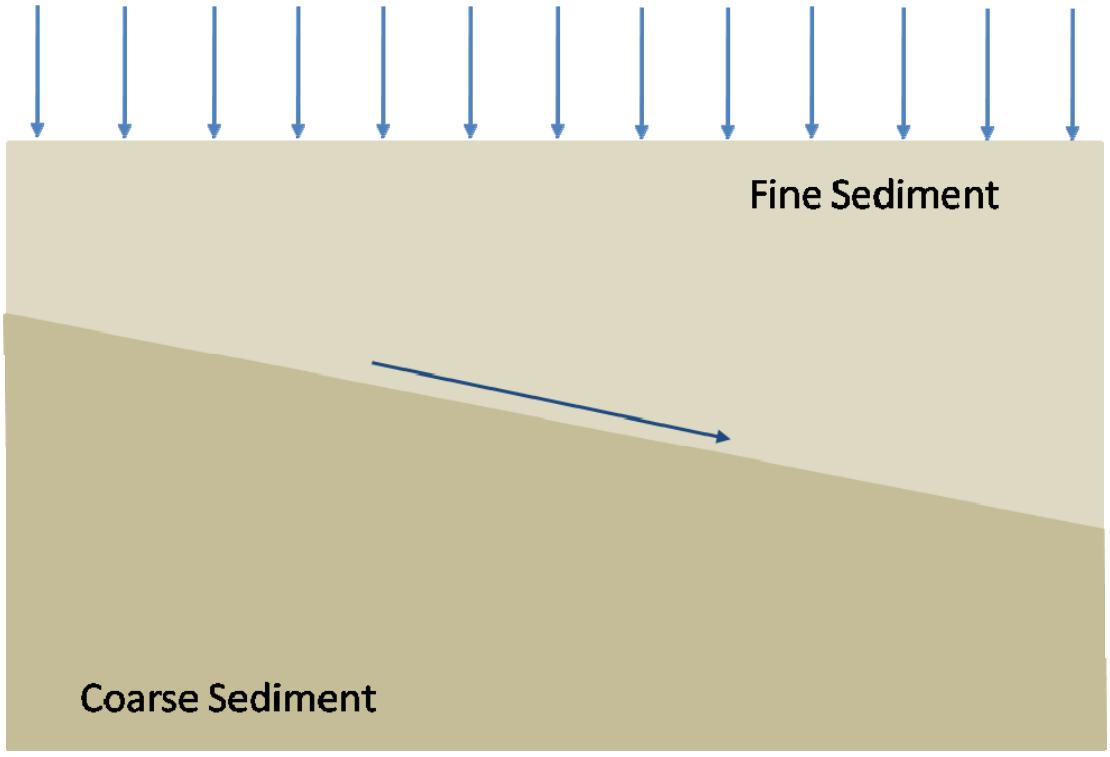

Figure 1. Schematic of capillary barrier system

Chapter 2: Literature Review

The following review of the literature provides background on capillary barriers and describes related experimental studies, modeling of capillary barriers, and dry regime infiltration mechanisms.

2.1 Background on Capillary Barriers

The use of capillary barrier systems (also known as Richards' barriers and soil covers) in the prevention of acid mine drainage and landfill leachate is ideal, due to their relatively low cost, long lifespan, and the preexisting sloping interface. Layering of fine over coarse material limits the infiltration of both water and oxygen and thus changes redox conditions, significantly reducing the potential for acid mine drainage (Weeks et al. 2004; Yanful et al. 2006) and mobilization of disposed hazardous materials (Kampf et al. 2003). Capillary barriers have also been proposed for use in long-term nuclear waste repositories as a secondary containment for spent-fuel storage. Carter and Pigford (2005) highlight the low cost, simple design, and robust safety features as reasons why the design is optimal for high-level waste repositories.

Due to the need for reliability and long-term durability, multiple experimental (Conca 1999; Porro 2001; Smesrud and Selker 2001; Kampf et al. 2003; Tidwell et al. 2003) and numerical (Oldenburg and Pruess 1993; Weeks et al. 2004; Yanful et al. 2006) studies have been conducted to assess the impact of infiltration and soil properties on capillary barrier stability. Ross (1990) first developed a constitutive relationship for

capillary barrier diversion capacity and diversion length using relative permeability-saturation relationships. The mathematical diversion capacity and length are defined by Ross (1990) as follows:

$$Q_{\max} > \frac{K_s \tan\phi}{\alpha} \qquad (1)$$

$$L < \frac{K_s \tan\phi}{q\alpha} \qquad (2)$$

where Q_{max} = the diversion capacity
L = the effective length
K_s = the saturated conductivity of the fine-grained layer,
ϕ = the down dip layer,
α = a soil property parameter, and
q = the infiltration velocity.

Steenhuis et al. (1991) further specified that breakthrough would not occur until pressures in the overlying layer reached the air entry pressure of the underlying layer, which was not explicitly stated by Ross' theory. Webb (1997) expanded Ross' work to include numerical methods and the two-phase van Genuchten characteristic curves. Smesrud and Selker (2001) extended Webb's work to provide guidelines for hydraulic properties using Miller and Miller (1956) scaling relationships, indicating that material between 2.5 and 5 times coarser (using average diameters) than the overlying layer would provide a functioning capillary barrier system.

2.2 Experimental Studies

Experimental studies of capillary barrier systems have been conducted to examine their overall performance and stability and to validate their associated theoretical and

numerical models. Under field-scale conditions, Porro (2001) studied the impact of yearly rainfall cycling and extreme wetting on a field-scale capillary barrier system and found that snowmelt and resulting high infiltration was the cause of capillary barrier failure. Kampf et al. (2003) performed large-scale laboratory tests to investigate discrepancies between barrier systems and numerical models. They found that under slow percolation, water was laterally diverted, but under high flow the seepage was irregular exhibition fingered flow which caused breakthrough. When compared to experimental investigations, they found the numerical model to be highly sensitive to the small changes in the hydraulic properties of the soils.

Conca et al. (1998) and Tidwell et al. (2003) examined the use of capillary barrier systems to divert water from high-level nuclear waste containers at a laboratory scale. The former used a crushed tuff overlaid by a silty sand with a 10-degree sloping interface to study the diversion capacity of a capillary barrier system by increasing the flow rate until failure was achieved. Experiments under these conditions matched Ross' diversion capacity relationship adequately. Long-term infiltration experiments were also conducted to examine steady-state conditions and slow infiltration of water into the gravel layer was observed. Upon conclusion of a 12-month test, Conca et al. (1998) observed moisture penetrating into the gravel several grain diameters across and hypothesized that this was potentially due to the capillary pressures of both layers being equal at the fine/coarse interface. Conca et al. (1998) also theorized that infiltration may be due to vapor diffusion. Using electrical conductivity, they

measured the increase in fluid content into the coarse material over a period of 12 months and found a water content of 6% and a diffusion coefficient of $10^{-11}cm^2/s$. Although calculations were performed, no final conclusions regarding the driving mechanism were made. Tidwell et al. (2003) constructed a capillary barrier with crushed tuff overlaid by Overton sand at a 30-degree sloping interface. The test liquid was composed of deionized water, conservative blue dye, and potassium iodide salt. Similar to Conca et al. (1998), Tidwell et al. (2003) observed breakthrough shortly after the fluid reached the coarse/fine interface, and infiltration to the center of the barrier system (where an emplaced waste container would be situated) 92 days into the experiment. Based on the retardation of blue dye and potassium iodide salt, Tidwell et al. (2003) suggested that the infiltration was due to a combination of adsorptive and diffusive processes. Although both Conca et al. (1998) and Tidwell et al. (2003) observed infiltration, it was of a significantly larger magnitude in Tidwell et al.'s experiment; this difference may be due to varying slopes and thickness of the overlying layer.

Site-specific requirements lead to significant variations in capillary barrier design and the resulting flow processes. Due to the varying configurations, little consensus on complex flow dynamics has been gained; up to this point the primary emphasis has centered on using numerical models as tools to design capillary barrier systems and not anomalous flow behavior.

2.3 Modeling of Capillary Barriers

Extensive modeling of capillary barrier systems has provided a wealth of literature on numerical methods associated with diversion systems. Beginning with theory developed by Ross (1990), numerical methods have been used to estimate diversion capacity and stability over diversion length. As with most unsaturated systems, numerical models used in capillary barrier systems adopt the Richards' equation, using van Genuchten (1980) or Brooks and Corey (1964) to estimate soil parameters. These models include HYDRUS (Zhang et al. 2009), TOUGH2 (Oldenburg and Pruess 1993; Wu et al. 2002), and ADIPIT (Weeks et al. 2004). Early modeling by Oldenburg and Pruess (1993) used TOUGH 2 to examine the extension of quasi-linear matric potential-hydraulic conductivity relationships to Ross' solution and investigate fluid breakthrough. Results indicated that breakthrough occurred gradually as the capillary pressure in the overlying layer became less negative and water was accepted by the underlying layer. Most recently Zhang et al. (2009) used HYDRUS 1-D to examine the potential importance of hysteretic and non-hysteretic soil when compared with experimental results. Zhang et al. (2009) found that highly hysteretic soils tended to have a lower moisture content in the upper layer than soils modeled without hysteresis, and models using hysteresis matched experimental breakthrough more accurately. Current modeling platforms provide a stable base for estimating capillary performance, but tend to fail when estimating breakthrough times at high fluxes (Zhang et al. 2009) and low saturations (Or and Tuller 1999). As

described by Or and Tuller (1999), most current models use a bundle of cylindrical capillaries or approximations of the Richards' equation where a pore is either empty or full, neglecting the impact of other flow processes such as vapor diffusion or water film flow. As with all dry regime systems, the use of more rigorous multiphase modeling software may aid in improving the reliability of capillary barrier models.

2.4 Dry Regime Infiltration Mechanisms

Results from capillary barrier experiments and numerical modeling indicate that much is still unknown about the behavior of water in capillary barrier systems. Both Conca et al. (1999) and Tidwell et al. (2003) note that the failure of their capillary barrier system may be due to dry regime flow processes, such as (1) vapor diffusion and (2) film flow. Both vapor diffusion and water film flow impact flow behavior, but are typically neglected because the impacts are often small and difficult to quantify and implement numerically. However, under specific circumstances these flow processes can dramatically impact the system behavior. Both vapor diffusion and film flow contributions to infiltration will manifest themselves in a similar manner in which infiltration distance (x) vs. time (t) is described by the Washburn relationship where $x \sim t^{1/2}$ (Bico et al. 2001) and are therefore difficult to decouple. The remainder of this discussion is dedicated to the roles of vapor diffusion and film flow as transport mechanisms in the dry regime, because of their potential impact on capillary barrier systems.

Water vapor diffusion in soil occurs when gradients in vapor pressure develop because of differences in temperature, salt concentration, and/or moisture content. The traditional equation for diffusion in soil is represented by Fick's law:

$$J = -D\frac{\partial C}{\partial x} \qquad (3)$$

where J = the flux of water vapor,
C = the concentration of water vapor,
D = the diffusion coefficient for water vapor, and
x = the distance across which the vapor concentration gradient exists (Jabro 2009).

According to Hillel (1998), vapor pressure gradients under isothermal field-saturated conditions are likely to be small when soils are nearly vapor saturated at all times. However, under very dry conditions, such as initial imbibition into a capillary barrier and where thermal gradients occur, significant variations in vapor pressure may develop.

Vapor diffusion is theoretically described by two terms, a diffusion coefficient and the gradient of concentration. In porous media, the diffusion term represents the resistance opposing motion and is also therefore a function of the actual porous media (Corey and Logsdon 2005). Bear (1972) (via Corey and Logsdon 2005) amended the traditional Fick's law to account for the media geometry and tortuosity:

$$J_i = -D_i^F \varphi \left(\frac{L}{L_e}\right) \nabla C_i \qquad (4)$$

where J_i = the flux of water vapor,
$D^F{}_i$ = the diffusion coefficient for water vapor,

φ	=	porosity,
L	=	direct distance between two points,
L_e	=	length of flow path, and
∇C	=	water vapor gradient,

which provides for a diffusion term that is media independent.

Occasionally, a chemical potential term is used to define a driving gradient (Nitao and Bear 1996); however, this approach is only valid under conditions of static pressure. Chemical potential in a multi-component system is defined by Atkins and DePaula (2006) as the sum of the total Gibbs free energy of a mixture with respect to the chemical constituent of interest. In terms of natural porous media, Nitao and Bear (1996) define the chemical potential as the sum of long-range and short-range potential energies by the following derivation:

$$\Delta U = -\Delta W_{LR} - \Delta W_{SR} - p\Delta\mathcal{U} + T\Delta S \quad (5)$$

where, the equation components are defined as:

$$\Delta W_{LR} = -\Phi_{LR} \quad \text{and} \quad \Delta W_{SR} = -\Phi_{SR} \text{ and, (6a and 6b)}$$

$$\Phi = \Phi_{SR} + \Phi_{LR} \quad (7)$$

Where	ΔU	=	the change in internal energy,
	ΔW_{LR}	=	the work done by long-range forces,
	ΔW_{SR}	=	the work done by short-range forces,
	$p\Delta U$	=	the work done by expansion,
	$T\Delta S$	=	the specific heat of the system, and
	Φ	=	the chemical potential of long- and short-range forces.

Therefore, the total energy in the system is equal to

$$\Delta U = \Phi - p\Delta\mathcal{U} + T\Delta S \quad (8)$$

Chemical potentials have been to used to determine the gradient for diffusion in porous media systems; however, as noted above, Corey and Logsdon (2005) emphasize that this is only relevant for a system with fixed pressure and temperature, as is made clear by the derivation above. Typically, dynamic hydrologic systems are poorly suited for this type of analysis; however, by keeping the limitations in mind, a chemical potential approach provides an understanding of end member conditions within a system. If we are careful, we can then use the derived equations to quantify potential capillary condensation caused by vapor diffusion under equilibrium conditions.

Capillary condensation is a process by which multiple layers of a vapor phase are adsorbed on the surface of a porous medium to the point where the pore space between opposing surfaces becomes filled with the condensed vapor. This process occurs due to the van der Waals and DLVO interaction inside the confined pore space: as surface forces attract the water vapor, the region is locally saturated and the vapor transitions to the liquid phase (Muller 1998). Derjaguin and Churaf (1974) illustrate that by combining the Kelvin and Laplace equations, a relationship between vapor pressure and slit width can be derived:

$$\left(\frac{RT}{v}\right)\ln\left(\frac{p_o}{p}\right) = \Pi(h) = \frac{2\sigma}{H} \qquad (9)$$

where R = the gas constant,
T = the temperature in Kelvin,
v = the molar volume of liquid,
p_o/p = the relative vapor pressure of the system, and

$\Pi(h)$ = the disjoining pressure,

which is equal to the capillary pressure (Muller 1998; Churaev 2003). Philip (1977) extended this equation to examine parallel plates, tubes, cylinders, and wedge-shaped pores by defining the capillary or matric potential of a soil as the sum of the adsorptive and capillary components. Philip's unitary approach provided the necessary mathematical foundation for the analysis of capillary pressure under a variety of geometries. Tuller and Or (1999) used a combination of Derjaguin and Phillip's mathematical derivations to apply a combination of the Kelvin and the augmented Young-Laplace equations to natural porous media. The resulting analysis produced simplified mathematical relationships for the hydraulic properties and configuration of adsorbed water in natural pore space as a function of surface area and geometry.

Additional studies and theory developed by Christenson (1994), Iwamatsu and Horii (1996), Hsieh and Wang (1997), and Muller (1998) have aided in the understanding of capillary condensation in porous media. However, their results are highly theoretical and outside the scope of the discussion for this review.

Conca and Wright (1990) and Jabro (2009) experimentally determined vapor diffusion rates for water into multiple different sediments over a range oftemperatures, saturations, and relative humidities. Conca and Wright (1990) found that diffusion coefficients decreased with increasing soil water contents. Values for basalt gravel and quartzite gravel varied from 1-100 $x10^{-9}$ cm^2/s. Jabro (2009) found

that the diffusive flux of water vapor increased with aggregate size and adsorption increased with temperature. Both studies provide an estimate for expected diffusion coefficients in soil systems.

The potential for a breach of the capillary barrier system drives our interest in vapor diffusion and capillary condensation. Under steady-state conditions, with a constant reservoir and high surface area sediments, it is theoretically possible for vapor diffusion to saturate the surface of sediments allowing for a hydraulic connection with the fine layer and causing the barrier to breach.

Water film flow is the second potential dry regime process that may lead to failure of capillary barrier systems. To fully understand water film flow into unsaturated media it is necessary to examine the relationship between surface roughness and wettability. On an interfacial scale, the movement of a liquid on a solid surface is determined by a balance of the surface tension forces, also commonly expressed by Young's equation:

$$\gamma_{SA} = \gamma_{SL} + \gamma cos\theta \qquad (10)$$

where γ_{SA} = the solid-air interfacial tension,
γ_{SL} = the solid-liquid interfacial tension, and
γ = the air-liquid interfacial tension.

Figure 2 illustrates the surface tension force balance on an idealized wetting surface and a moderately wetting surface (Quere 2008).

When natural surface roughness is introduced, the wettability is altered by changes in the contact angle (Wenzel 1936). Wenzel first introduced the relationship between

increased hydrophobicity or hydrophillicity and surface roughness where the amended contact angle is represented as follows:

$$\cos\theta^* = r\cos\theta \qquad (11)$$

where θ^* is the contact angle on a rough surface and r is a roughness coefficient. Figure 3 illustrates the relationship between surface roughness and an advancing fluid front. In practice this mathematical representation only provides a guideline, because it is difficult to isolate the r and Θ* values (Martines et al. 2005). Cassie and Baxter (1944) developed a relationship where they assume that the air is trapped within surface divots so the fluid sits on top of both the surface and air. This is described as follows:

$$\cos\theta_{CB} = r_f f\cos\theta_Y + f - 1 \qquad (12)$$

where θ_{CB} = the Cassie-Baxter contact angle,
r_f = the roughness factor of the wetted area,
f = the area fraction of the wetted area, and
θ_y = the ideal contact angle.

Both of these equations describe a system at equilibrium; however, at slow speeds they may be extrapolated to dynamic systems (Martines et al. 2005).

Hay et al. (2008) outlined three primary phases of water film infiltration into porous media: precursor film flow, roughness invasion, and reaction to the external forces. The precursor film is driven forward by local advective water vapor transport and the formation of a macroscopic meniscus on the edge of the invading front. Although not stated explicitly in the literature, it is likely that capillary condensation is the driving

mechanism for mobilization. Following the precursor film is roughness invasion, which is driven by capillary forces and the surface geometry of the solid-liquid interface. The final stage of film movement is dominated by bulk flow and gravitational forces (Hay et al. 2008). Using the term hemi-wicking, Quere (2002) described the process by which fluid is drawn across a rough surface, moving from a drop to a thin film. Quere (2002) presented the traditional thermodynamic representation of surface forces as follows:

$$dE = \left(\gamma_{SL} - \gamma_{SV}\right)\left(r - \phi_s\right)dz + \gamma_{LV}\left(1 - \phi_s\right)dz \tag{13}$$

Where dE = the change is surface energy,
γ_{SL} = the solid liquid interfacial tension,
γ_{SV} = the solid vapor interfacial tension,
r = the roughness,
ϕ_s = the surface area of the sample, and
γ_{SV} = the liquid vapor solid liquid interface.

In systems in equilibrium dE = 0. When viscous forces dominate over inertial forces, the film mobilization is expected to follow a diffusion type relationship, also known as a Washburn law (Quere 2002).

Within the field of material science, multiple experiments have been conducted to control the wettability of materials using surface roughness (Bico et al. 2001; Bico et al. 2002; Ishino et al. 2004; Martines et al. 2005). For example, Martines et al. (2005) illustrated that the movement of fluid across the surface of fabricated nanopatterns could be predicted by hemi-wicking theory and the Cassie-Baxter equation by using patterns and surfaces separated by distances smaller than the capillary length to

channel the flow and alter the wettability of a material (Martines et al. 2005; Quere 2008). When comparing surface geometry to the Cassie-Baxter equation, Martines et al. (2005) found good agreement.

Bico et al. (2001) extended this theory to the study of porous media where they examined the movement of an infiltrating film across a rough surface from a reservoir . They compared theoretical imbibition dynamics to infiltration of silicon oil by using a fabricated surface geometry. As expected, the imbibition followed a diffusion law, and by balancing the viscous forces with a diffusion law the following equation was derived:

$$z = \left(\frac{2}{3\beta} \frac{cos\theta - \cos\theta_c}{\cos\theta_c} \frac{\gamma\delta}{\eta} t \right)^{1/2} \qquad (14)$$

where z = the infiltration distance,
β = a fitting parameter,
θ_c = the critical contact angle where imibition will occur,
γ = the surface tension,
δ = the depth of the roughness, and
η = the viscosity.

Bico et al. (2002) then considered the impact of surface roughness on capillary rise in a roughened capillary tube and found two wetting fronts, an initial precursor film over roughened side walls and a cumulative increase in bulk capillary rise. Their studies concluded that for hydrophilic materials fluid spreads across the solid texture or across the topography of the surface, moving until the fluid contact angle has reached its theoretical value, θ^*. This was further studied by Quere and Bico (2003) where

the impact of the precursor wetting film was found to be a driving force for fluid movement (or wicking) into larger pores in porous paper materials.

Hay et al. (2008) provided a geometric model for surface roughness relevant to natural porous media; by adding in a term for the hydraulic diameter to obtain the following average invasion velocity:

$$U = \frac{\gamma d_h^2}{2Po\mu x}\left(\frac{(2\delta + \lambda)cos\theta - \lambda sin\theta}{\delta\lambda}\right) \qquad (15)$$

where
- U = average infiltration velocity,
- γ = the surface tension,
- d_h = hydraulic diameter,
- Po = poiseuille number,
- μ = viscosity,
- θ_c = the critical contact angle where imibition will occur,
- δ = the amplitude roughness, and
- λ = the wavelength of the roughness

Hay et al. (2008) also considered multiple other approximations for fluid configurations in natural geometries, including the Poiseuille film flow approximation and Hagen-Poiseulle half-pipe approximation. Comparison to Bico et al. (2001) experimental results indicated that the hydraulic diameter approximation fit infiltration of the silicon oil the best.

Alongside these efforts in the field of material science, similar studies of surface roughness, water film movement, and water film flow hydraulics have taken place in the field of hydrology (Nitao and Buscheck 1991; Tokunaga and Wan 1997; Or and Tuller 1999; Or and Tuller 2000; Tokunaga et al. 2000; Pismen 2001; Tokunaga and Wan 2001; Tokunaga and Wan 2001; Jones and Or 2002; Liu 2004; Culligan et al.

2005; Tuller and Or 2005; Tokunaga 2009). Much of the motivation for examining film flow in the dry regime was initiated by the need to understand water movement in Yucca Mountain fractures and the anomalous presence of chlorine 36 in groundwater under the Yucca Mountain site (Tokunaga 1997).

Tokunaga and Wan (1997) experimentally studied water films over a range of matric potentials and determined the transmissivity, hydraulic conductivity, and average film thickness for water held in Bishop tuff. They concluded that film flow is most likely a contributing (but not a dominating) component of the total fluid flux. Follow-up studies by Tokunaga et al. (2000) used a Green and Ampt (1911) model for film infiltration and hydraulic diffusivity of a rough glass surface. Infiltration was quantified by measuring the movement of a wetting front over a rough surface as a function of time from an open reservoir. Infiltration velocities were then fitted to a Green and Ampt style equation to determine a film diffusion coefficient. In subsequent work, Tokunaga and Wan (2001a, 2001b) isolated the relative flux contributed by the surface fracture flow when compared to matrix flow in a Topopah Spring welded tuff and an Owens Gorge rhyolite. In contrast to their earlier findings (Tokunaga and Wan 1997), in 2001 they determined that surface fractures and film flow can contribute a significant flux when the surfaces of a rock have a higher permeability than the matrix. Flow regime boundaries were also isolated using the Young-Laplace equation to define a range of matric potentials where fast film flow can be expected. More recently, Tokunaga (2009) presented theories on the flow

hydraulics of water films in porous media and how adsorption can potentially impact fluid flow. These studies indicated that film viscosity and conductivity are impacted by the adsorptive forces between films and sediments.

Parallel studies conducted by Tuller and Or (Or and Tuller 1999; Tuller et al. 1999; Or and Tuller 2000; Tuller and Or 2001; Tuller and Or 2005) provide similar theoretical and mathematical descriptions of water films in porous media. Early adsorption studies referenced previously (Tuller et al. 1999) led to examination of the spatial arrangement of liquid in pore space with regard to specific geometries (Or and Tuller 1999). Much of the emphasis of the 1999 Or and Tuller paper is on upscaling theory and outside the scope of this investigation; but subsequent study (Or and Tuller 2000) of surface roughness and hydraulic conductivity provide a statistically derived average hydraulic conductivity using geometric relationships for curves, corners, and pits of porous media surfaces. When compared to results from Tokunaga and Wan (1997), the relationship of surface roughness to hydraulic conductivity was in good agreement. Finally, Tuller and Or (2005) used adsorption isotherms to relate sediment surface area to the low end of soil water characteristic curves, indicating (not surprisingly) that the presence of films on the low end of the soil water characteristic curve is dictated by adsorptive van der Waals forces and not by capillary forces.

Although studies conducted in the fields of materials science and hydrology may appear to be similar, it should be noted that researchers in materials science are

interested in the film infiltration velocity, whereas hydrologists have focused on the hydraulic conductivity of already-existing films. For the purpose of understanding the initial capillary barrier breach in dry systems, film infiltration velocity provides more relevant information than studies of unsaturated flow in porous media.

This review presents a summary of capillary barrier flow behavior and associated theory, followed by a discussion of two major components not traditionally considered in modeling and design of barrier systems. By reviewing past experiments, specifically those of Conca et al. (1998) and Tidwell et al. (2003), we have illustrated that traditional design theory does not fully account for flow processes in dry capillary barrier systems, but provides two dry regime flow processes as an explanation for capillary barrier failure. Both vapor diffusion and water film infiltration into unsaturated sediments follow a Washburn relationship, and are therefore difficult to decouple. However, diffusion coefficients derived by Conca and Wright (1990) are dramatically slower than the diffusion rate in experiments conducted by Tidwell et al. (2003), indicating that film flow is likely a controlling factor. In the following manuscript (Chapter 3), we will examine the relative impact of these two processes in the context of two capillary barrier experiments conducted for materials and conditions similar to those of Tidwell et al. (2003).

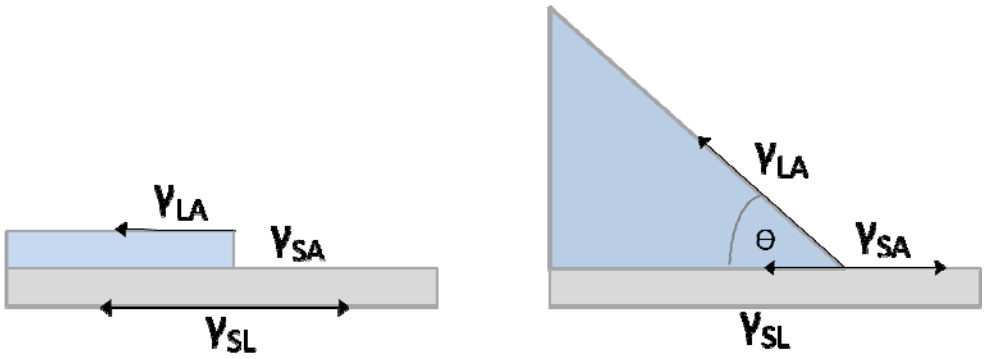

Figure 2. (Left) A liquid film with a high solid-liquid interfacial tension and low contact angle; (Right) partial wetting and balance of surface tensions (Figure adapted from Quere 2008)

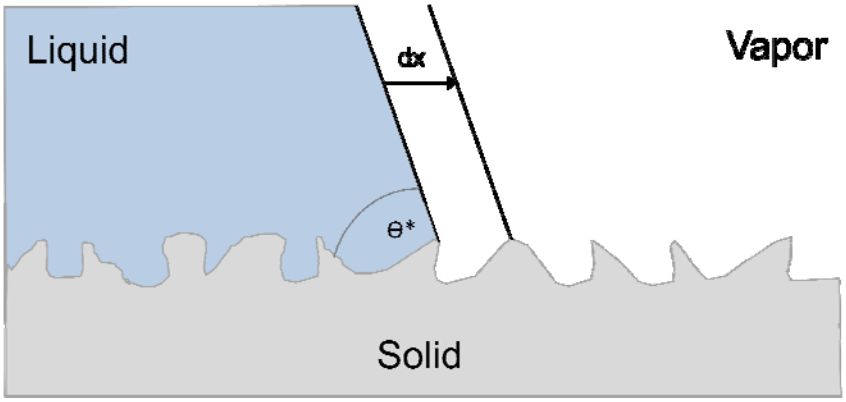

Figure 3. Film invasion onto a rough surface

Chapter 3: Flow Processes in the Dry Regime: The Effect on Capillary Barrier Performance

D.P. Jansik, D. Wildenschild, and N.D. Rosenberg

To be submitted to Vadose Zone Journal

3.1 Introduction

Computer simulation models have become essential tools for quantifying the physical processes associated with the near-surface environment in almost any scientific or engineering effort involving water resources. However, the reliable application of these computer models depends on the acquisition of representative physical soil properties and an understanding of underlying physical processes. It is ordinary practice to assume that the estimated van Genuchten (1980) or Brooks-Corey (1964) parameters adequately represent our materials in a hydrological sense. Nevertheless, material properties, such as grain morphology and surface roughness, can have a significant influence on the flow and transport properties of a porous media.

Under the study reported here, we present an example of the impact of grain morphology and surface roughness on predicting capillary barrier system efficiency, highlight inconsistencies in modeling, and discuss dry regime flow processes. Standard laboratory measurements of hydrologic properties were used to select two coarse gravels for the underlying layer in the two capillary barrier systems. Although van Genuchten parameters fitted to measured retention characteristics indicated that the two materials were hydrologically similar, they behaved differently under experimental conditions. We believe this is due to the significantly different surface areas and geometries of the two sediments.

By ignoring dry regime processes such as (1) film flow and (2) vapor diffusion, we were unable to accurately model water flow within the sediment. However, once film

flow and vapor diffusion were included in the analyses, we could more successfully explain the observed behavior. The significance of the film flow component was found to be highly dependent on the surface roughness, with film infiltration velocities increasing with surface roughness and wettability. The concepts discussed are not limited to the conditions associated with a capillary barrier; they apply to many aspects of modeling unsaturated flow and transport in porous media in the dry regime.

Both film flow and vapor diffusion impact fluid flow in the dry regime, but they are typically neglected because their impacts are often small and difficult to quantify. However, under specific circumstances these dry regime flow processes can dramatically impact the system behavior. Studies conducted by Hu et al. (2004) examined the impact of water content and thin water films on the movement of a solute through crushed tuff and found solute mobility to be a function of water film thickness and continuity. The presence of water films impacted the rate of diffusion within the system and the interconnectedness of pore space. In a similar capillary barrier system, and using the same materials as used here, Tidwell et al. (2003) observed equivalent breakthrough into coarse sediment, at an initial rate of 20% later slowing to 10% of the infiltrating fluid. The fluid breakthrough was attributed to water film flow and/or vapor transport.

Film flow and vapor diffusion contributions will manifest themselves in similar manner, following what is known as a Washburn relationship where $x \sim t^{1/2}$ (Bico et al.

2001), and are therefore difficult to decouple. The present work is focused on elucidating which mechanism is the dominant driver for these particular experiments. By using the theoretical relationships relating surface roughness to infiltration velocity developed by Hay et al. (2008) and qualitatively investigating theoretical vapor flux, we were able to isolate the primary mechanism for capillary barrier breach.

The capillary barrier experiments presented here also provide an ideal example for analysis of discrepancies between ideal models and experimental system complexities; a traditional model used here failed to predict the observed capillary barrier performance. It should be noted that, this capillary barrier design has the potential to be considered for high-level waste containment systems in which a capillary barrier would be established between the two different materials and water would be diverted away from the sensitive materials, such as vitrified glass or cement waste forms. These systems can also be used as diversion systems under less rigorous operating conditions.

Film Flow

Film flow in unsaturated sediments has been described in many studies (Tokunaga 1997; Tokunaga et al. 2000). Tuller et al. (1999) and Tuller and Or (2001) pointed out that many models neglect film flow aspects by assuming that flow occurs only in full capillaries. Thus, the pressure potential is attributed to capillary forces only, while other potentially important adsorptive surface forces are ignored. This

simplified model representation often provides satisfactory results for intermediate and highly saturated media, but, they tend to fail at low saturation (Nimmo et al. 1994).

To quantify the relative contribution of film flow in these systems we used knowledge of the sediment geometry, roughness and the theoretical expression of Hay et al. (2008). Wenzel (1936) first conceptualized the impact of surface roughness on wettablity and contact angle. Since then, extensive research has been conducted to quantify the effect of roughness on solid wetting and water film flow (Bico et al. 2001; Bico et al. 2002; Quere and Bico 2003; Martines et al. 2005; Hay et al. 2008). Hay et al. 2008 coupled surface geometries with the movement of water films to produce a conceptual model providing a pseudo sorptivity (or diffusion) term of water film infiltration velocities using only contact angles, surface tension, viscosity, and the sediment surface geometry.

Vapor Diffusion

DiCarlo et al. (1999) suggested vapor pressure gradients as a mechanism for enhanced movement of liquid and thus could account for differences in lateral spreading of moisture fingers observed in experiments. The vapor diffusion approach was based on the conservative assumption that the unsaturated hydraulic conductivity contribution to the sum of liquid and vapor transport (eq. 2 in DiCarlo et al. 1999) is extremely small at very low fluid saturations, and also that the vapor condenses to liquid behind the vapor front even in the absence of a temperature gradient. The latter

assumption is supported by many studies showing that under equilibrium conditions vapor will condense, i.e., adsorb to porous materials, even though the porous material has the same temperature as the vapor. Parker (1986) explains that when a dry hydrophilic porous medium is placed in an atmosphere containing water vapor, isothermal water adsorption will increase with increasing vapor pressure until the pore space becomes fluid-filled. Similarly, Kutilek and Nielsen (1994) stated that the nature of soil water adsorption through hygroscopicity is completely different from the simple process of vapor condensation to its liquid phase. The adsorption phenomena are generally classified as being either physical (based on electrostatic and van der Waals attraction forces between the solid surface and water molecules) or chemical (based on rearrangement of electrons and consequent formation of strong chemical bonds) (Parker 1986; Nitao and Bear 1996). The adsorbed water layers coating the solid grains grow into films, and eventually adsorbed films in adjacent pore spaces will coalesce and form a continuous liquid phase in the pore. This process is generally referred to as capillary condensation (Derjaguin and Churaf 1974; Tuller et al. 1999). According to Easton and Machin (2000) there is no well-defined limit to the amount of vapor that can be absorbed for a wetting fluid; however, Tokunaga and Wan (2001) suggest that water films range in thickness from tens of nanometers to ~1μm. The adsorption of water vapor is aided by the vapor pressure deficiency that exists over a concave surface (air-water meniscus in a pore) compared to the vapor pressure over a free, flat water surface (Bear 1988).

In sharp contrast, Hu et al. (2004) report that Conca (1990) found that four sizes of tuff gravel remained dry after equilibrating for 70 days in a nearly 100% relative humidity. At the conclusion of the experiment only a 2.7% increase in intergranular water content was observed, indicating that the relative importance of vapor diffusion for water infiltration may be minimal.

Vapor diffusion enhancement could contribute to the observed infiltration into the underlying layer in these experiments, but it is generally considered to only occur where a temperature gradient is present (Cass et al. 1984; Wildenschild and Roberts 2001). However, Webb and Ho (1998) reported both experimental and numerical modeling evidence of the enhancement of vapor diffusion in the absence of a thermal gradient. According to their study, the vapor density gradient, which drives the enhancement, can be established without the influence of a thermal gradient, for instance due to a vapor concentration gradient. In either case, enhancement across liquid bridges in the coarse material is a possible, but a fairly unlikely explanation, because at the saturation at which liquid islands develop in the coarse sand, the saturation level will also be sufficient to support capillary action, which is a much more efficient transport mechanism.

Thus the question remains, what is the relative impact of vapor diffusion or water film infiltration in unsaturated systems? It is likely that both processes are occurring simultaneously. The following experiments are targeted at understanding the importance of dry regime flow processes in a working capillary barrier system.

3.2 Experimental Design

The following sections describe the materials, surface area analysis, associated hydrologic parameters, and laboratory setup for the capillary barrier experiments.

Materials

Under our study, we conducted two experiments using commercially available Overton fine silica sand (#50–70 sieve) as the fine material and either 8/20 angular sand (#8–20 sieve) or 2/16 rounded sand (#2–16 sieve) as the coarse layer. The two experiments are referred to as Experiment 1 and 2, respectively. The coarse material for Experiment 1 was selected according to its utility as future backfill for the potential Yucca Mountain waste repository, thus a coarser crushed volcanic tuff was obtained from a supplier local to Yucca Mountain. For Experiment 2, sand with a similar grain size distribution was used, but we chose a material with a lower surface area and more rounded grains. The particular type of fine-grained material was selected because it would not filter into the coarse-grained material under dry conditions. See Table 1 for additional details about material properties.

Surface Area Analysis

Specific surface areas for the two coarse sands were measured using the Brunauer-Emmett-Teller (BET) (Brunauer et al. 1938) technique. The materials were out-gassed at room temperature to prevent sintering at high temperatures. Both total surface area and micropore area were measured in duplicate measurements and the results are listed (as averages of the measurements) in Table 1. As seen in Table 1,

the 8/20 angular sand has 10 times higher total area than the 2/16 rounded sand. The 8/20 micropore area alone amounts to the total surface area for the 2/16 rounded sand. Figure 4 shows microscopic photos of the two materials, and the difference between the two is quite noticeable. The 2/16 rounded sand consists of a very uniform quartz sand of very rounded grains, whereas the 8/20 angular sand is a volcanic tuff consisting of very angular grains containing various minerals and exhibiting intra-granular porosity.

Another difference between the two coarse materials is their grain morphology or angularity, and resulting pore shapes. Tuller et al. (1999) show in their Figure 4 that pore space geometry (the pore shape and angularity of grains) has a marked influence on the imbibition and drainage processes. During imbibition, the liquid-vapor interface in corners of angular pores grows with increasing potential (or capillary pressure) to the point of snap-off, whereas the round pores go from being completely empty to being full without the intermediate steps that occur in angular pores. Though both sediments in this system produced angular pores space, the angular 8/20 angular sand, produced more jagged edges and irregular pore space shape. Under drainage conditions, liquid displacement in cylindrical pores is piston-like, whereas in angular pores the liquid is displaced from the central region first leaving liquid in the corners. Subsequent increases in capillary pressure result in decreasing amounts of liquid in the corners (Tuller et al. 1999).

Hydrologic Parameters

The hydrologic characteristics of the materials were measured separately in smaller sample holders. The retention characteristics were measured using a quasi-static approach (Wildenschild et al. 1997) in a smaller pressure cell (7.6 cm diameter, 3.5 cm long). Saturated hydraulic conductivity was measured in a column (2.5 cm diameter, 28 cm long) using the constant head technique (eg. Klute 1986) for at least three different hydraulic gradients for each sample, and the unsaturated hydraulic conductivity was derived from the retention data. The resulting retention and unsaturated hydraulic conductivity curves for all materials used are illustrated in Figures 5 and 6. A non-linear least-squares optimization routine (RETC version 6.0 from the U.S. Salinity Laboratory) was used to fit van Genuchten (1980) parameters (listed in Table 2) to the curves. The two coarse materials have very similar hydrologic properties, except for a noticeable difference in residual saturation (Table 2), and a small difference in air entry pressure; but compared to the fine layer (Overton sand) they are very similar.

Laboratory Setup – Capillary Barrier System

The capillary barrier experiments were carried out in a bench-top aluminum box (60.5 cm x 56.0 cm x 10 cm) with a Pyrex window on one side allowing easy detection of flow patterns (see Figure 7). Two 0.5-bar tensiometers were installed from the backside of the box (marked as squares in Figure 7). The tensiometers consisted of porous ceramic cups glued onto the backside of the box, and by testing

were confirmed to have an air-entry value of at least 250 cm prior to use. Drainage out of the box was achieved by the use of two stainless steel, sintered rods installed from the backside immediately above the fine/coarse interface (circles in Figure 7). These drains had relatively low air-entry values (< 70 cm), but were highly permeable, such that water flow out of the box was not inhibited. They were connected to water-filled tubing, providing hanging column-based water phase tension to facilitate drainage under less than fully saturated conditions. Temperature variations during the experiments were measured with four thermocouples (1.02 mm diameter) placed in the box as shown in Figure 7 (stars).

The sandy materials were packed loosely in the box to simulate the emplacement of sediment using a conveyor belt such as would potentially be used at Yucca Mountain. As expected, the porosities of the materials varied slightly between the loose packing of the experimental box and the packing in the smaller pressure cells that were used for the hydrologic property measurements, the latter generally having lower porosities. We assume that the porosities for the experimental box were associated with the largest error due to inaccuracies of the material weights (loss during packing, etc.) and difficulty in precisely estimating the geometric boundaries of the individual layers. Before the materials were poured into the box, it was tilted to a 24-degree angle so that the fine/coarse interface was horizontal during packing. Table 3 lists relevant information from the experiment. An infiltration device was placed on top of the box to provide uniformly distributed infiltration over the entire surface area of the

top of the box. A water-filled reservoir with 64 drips (0.25-mm inner diameter tubing and finger-tight fittings) was connected to a diaphragm pump. The pump rates were tested both before and after each experiment and are listed in Table 3. The average rate of infiltration into the underlying coarse layer for Experiment 1 was (29.8 – 27.8 ml/h) = 2.0 ml/h or 9.2 10^{-9} m/s, and for Experiment 2 only 0.1 ml/h (which is less than the standard error on the outflow rate) or 4.6 10^{-10} m/s. These numbers show that (assuming minimal or at least similar evaporation and other losses), the average infiltration into the coarse layer in the two experiments varied by a factor of 20. This calculation is a rough estimate, but provides a ballpark figure for the amount of fluid infiltration.

3.3 Results

The results of the capillary barrier experiments, associated numerical modeling and dry regime interpretation are described in the following sections.

Capillary Barrier Experiments

Infiltration and outflow rates for the two experiments are shown in Figure 8. Each box had an initial increase in outflow rate until steady-state flow conditions were established. In addition to infiltration and outflow rates, the average and standard deviations of the outflow rates are listed in Table 3. As seen in Figure 8, some water was retained in the box in Experiment 1 (Overton sand over 8/20 angular sand); the infiltration rate was higher than and exceeded one standard deviation of the average outflow rate. The drains diverted an average of 93.3% of the infiltrating water, which

means that on average, the infiltration front moved at a rate of 6.7% of the applied inflow rate. This compares reasonably to the approximately 10% to 20% of the applied rate that Tidwell et al. (2003) found. In Experiment 2, using the 2/16 rounded sand as the coarse material, the infiltration rate was within a standard deviation of the outflow rate and the amount of water being withheld in the box was within measurement error. The amount of water diverted in this case was 99.7%.

The drain suction and tensiometer readings for the two experiments were monitored throughout the experiment. The air-entry value of the lower tensiometer (placed in the initially dry coarse material) was exceeded during the initial wetting procedure for both experiments and thus no readings are available for the capillary pressure in the coarse material during the experiments. After an initial adjustment period, the drain pressure was almost constant throughout the first experiment (43.2 cm +/-1.5 cm), whereas the capillary pressure measured at the upper tensiometer (in the fine material) varied slightly more (32.9 cm +/- 2.8 cm). The more notable fluctuations in capillary pressure in the box were closely correlated to temperature variations in the box, and are attributed to the temperature sensitivity of the transducers. In the second experiment the upper tensiometer was also fairly constant, apart from temperature-induced variations (35.7 cm +/- 2.8 cm). In this experiment the average drain suction was 46.3 cm +/- 2.1 cm, which was very similar to Experiment 1. A ceramic plate (initially intended for drainage) functioned as an additional tensiometer during part of this experiment and, after the initial non-steady-state wetting period, the measured

capillary pressures were almost identical to the capillary pressures measured at the upper tensiometer. The upper tensiometer and the ceramic plate were located at a vertical distance of 21 cm from the base of the box and the fact that practically identical values were measured at both vertical locations indicates that flow had reached steady-state and was driven by gravity alone. The unsaturated hydraulic conductivity was thus equal to the flow rate through the box, providing us with measurement points on the unsaturated hydraulic conductivity curve for the Overton sand; these points are illustrated as individual points in Figure 6.

To better illustrate the flow patterns in the experiment, a dye tracer (Phenol Red) was sprinkled on the sand surface where it dissolved in the infiltrating water. In the first experiment it was added at the beginning of the experiment (initially dry sand), while in the second experiment it was added after 5 days when the wetting front had already reached the material interface. Phenol Red is a very conservative tracer with low adsorption capabilities. To document the tracer transport, images were periodically collected over the duration of the experiment. A time-lapse series of photographs for each experiment is shown in Figure 9 for Experiment 1 and 2, respectively. It is evident that in both experiments the water moved into the coarse layers and infiltrated faster (and further) into the 8/20 angular sand than into the 2/16 rounded sand. This is in agreement with the amounts of water diverted by the drains for the two experiments. Only 0.3 % of the infiltrated water was retained in the box for the second experiment (2/16 rounded sand as the coarse layer), whereas 6.7% was

retained in the box for the first experiment (8/20 as the coarse layer). Tidwell et al. (2003) used materials that were identical to our Experiment 1 and derived very similar results: the barrier effectively diverted the majority of the infiltrating the water, and similar to our results, they found a slow and continuous infiltration into the coarse layer (see their Figure 2), the onset of which was noticed almost immediately after the wetting front reached the capillary interface. At the end of each experiment, an industrial vacuum was used to empty the box of sand. Successive layers were carefully removed and samples (approximately 25 ml) were collected. The samples were weighed and placed in a 105 ^{o}C oven over night and subsequently weighed again to determine the water saturation. The wetting front had progressed approximately 14 cm into the 8/20 angular sand, whereas only a narrow band of approximately 2 cm was significantly wetted in the 2/16 rounded sand. By analyzing the photographs of the experimental box taken at regular intervals and scaling the infiltrated distance to a feature of known length in the image, we estimated the infiltrated distances as a function of elapsed time as illustrated in Figure 10. The infiltrated distance is plotted as a function of $t^{½}$, and it is obvious that the infiltration follows this relationship almost perfectly.

3.4 Numerical Modeling

We used the US1P module of NUFT (Non-isothermal Unsaturated-saturated Flow and Transport) (van Genuchten 1980; Nitao 1998) for the design simulations. This module solves the equations for single-phase unsaturated flow in porous media.

XTOOL, a NUFT postprocessor code, was used to display the output of the code in graphical form. Before simulating the experiments described here, we compared the results of a capillary barrier simulation with results reported in Webb (1997) to gain confidence in our ability to model capillary barriers using NUFT. Webb's (1997) solution was selected due to its incorporation of characteristic curves and prior accurate prediction of capillary barrier performance. The NUFT simulations were in excellent agreement with Webb's results.

The two-dimensional model domain for the experiments is shown in Figure 11. The hydrologic properties used in the simulations are given in Table 4. In our numerical model, we describe the relationship between moisture content, capillary pressure (i.e., suction, head), and permeability using the van Genuchten (1980) and Mualem (1976) expressions(Mualem 1976; van Genuchten 1980). NUFT input requires different parameters in some cases from those listed in Table 4. For example, NUFT uses the van Genuchten m where m = 1-(1/n). Also, NUFT uses saturations rather than moisture contents. Saturation, S, is defined as the moisture content, θ, divided by the porosity, ϕ. We assumed that $\theta_s = \phi$ (the porosity) in our simulations.

Initially, the sands were assumed to be completely dry. The top boundary and the drain were held at constant head and saturation. The infiltration rate and drain suction used in the simulations are also given in Table 4. As a test, simulations for Experiment 1 were done with approximately double the grid resolution with no significant difference in model results. Simulations for Experiment 1 and 2 were run

out to 33 days and 18 days, respectively, to match the actual length of the laboratory experiments.

3.5 Model Results

The saturation fields for Experiments 1 and 2 using the domain and grid shown in Figure 11 and the parameter values given in Table 4 are shown in Figure 12. As these figures clearly show, NUFT predicts successful performance of the barrier, and the complete absence of any wetting front migrating into the lower coarse material in both cases. However, a clear wetting front was observed for both cases in the actual experiments. The wetting front moved much faster and further into the 8/20 angular sand in the experiments, but because the two coarse materials have almost identical hydrological properties the model simulations predict nearly identical behavior for both experiments.

In attempting to capture the observed behavior with the numerical model, we adjusted various parameters to account for measurement error on the hydrologic properties. We used two principles to guide us with respect to which parameters we adjusted and by how much. The first was the likely bound of general parameter uncertainty. The second was the likely differences between the parameters determined from the drying curves we used to determine the values reported in Table 4 and the parameter values that we would have determined had we measured wetting curves rather than drying curves. In general, a wetting curve has a similar van Genuchten n-value but a greater α-value. For these experiments, wetting curves more likely represent the conditions

in the coarse sand. For the fine sand, it is more difficult to know which curve better represents conditions in the system; most likely the most representative values are somewhere in between those for the two curves.

Infiltration into the underlying coarse material was observed as illustrated in Figure 13 when the α, m, porosity, and saturated conductivity values were altered to the values listed in Table 5. Manipulation was required to match the experimental results; K_s was halved and α doubled for the fine sand; K_s was halved and m and the porosity were altered to varying degrees for the coarse sands. Even though we were able to reproduce the results seen in the experiments by adjusting the hydrologic parameters, it seemed unwarranted to blindly venture into an exercise of pseudo parameter estimation when the likely cause was the lack of consideration of dry regime flow processes. This reasoning is also supported by the fact that the difference observed between the two experiments using the different coarse materials is not captured in a quantitative manner (see Figure 13) by this parameter estimation exercise.

Figure 14 illustrates the pressure-saturation curve for the measured hydraulic parameters (solid line) and the curves for the parameters required to obtain a model fit (dashed line). Clearly, the changes required in the α parameter of the fine sand dramatically impact the expected hydraulic properties of the soil, bringing the average pore throat radius significantly closer to that of the 8/20 angular and 2/16 rounded sand.

3.6 Dry Regime Experiments

A traditional modeling approach yielded results that explained neither the breach of the barrier nor the differences between the two sediments; therefore, a number of alternative physical flow mechanisms must be considered. The numerical model predicts a perfectly working capillary barrier for both material combinations, unless the hydrologic property values are adjusted. This indicates that the wetting phenomena observed in the experiments are due to mechanisms not considered in traditional numerical simulations. Two different questions need to be addressed: 1) how do we account for the slow, but constant, wetting of the coarse layer, which happens near the fine/coarse layer interface in both experiments; and 2) why is there such a large variation in wetting front saturation level and depth for the two different coarse materials (despite the fact that they have very similar hydrologic properties)? We believe that the primary cause for infiltration in the two systems was flow processes specific to the dry regime. The increased infiltration in Experiment 1 was primarily caused by significantly higher surface area and a higher natural wicking action from the sediments. To further explore the impact of dry regime processes, supplemental experiments and data were collected to examine the relative roles of film infiltration and vapor diffusion. Because the dry regime processes were most clearly demonstrated in Experiment 1, the 8/20 angular sand was used for additional measurements of vapor diffusion.

Vapor Diffusion Experiments

Vapor diffusion into sediment samples was monitored gravimetrically. Ten grams of coarse sediment was dried at 105º C and placed in a sealed closed container with an open reservoir of water. Relative humidity was monitored using a portable relative humidity sensor and maintained near 95%. The change in the mass of the sediment sample was monitored over a period of 10 days using an analytical balance accurate to +/-0.001 g.

Sediment Surface Characterization

Surface profiles of the 8/20 angular sand were obtained using a Nanonics Multiview 1000 atomic force microscope system, with a 70-micron scanner in non-contact mode with a non-contact probe. Image analysis using WxSM image processing software was used to obtain the average amplitude (δ) and wavelength (λ) of sediment surface features.

3.7 Results of Dry Regime Experiments

The dry regime experiments illustrated that vapor diffusion onto sediment surface in the absence of a gradient was minimal. Over a period of 10 days the mass change in sediment weight was within the experimental margin of error of the analytical balance. As mentioned previously, similar findings were reported by Conca (1990), who determined the vapor diffusion coefficient for tuff gravel samples to be 10^{-15} m^2/s (or 8.6×10^{-7} cm^2/day). At the saturated fine/coarse material interface in the experimental system discussed here, the relative humidity would be expected to be

near 100%. Because the dry coarse material is overlain by wet fine sand, the relative humidity within the pore space of the coarse material would equilibrate within hours; therefore, we postulate that due to the lack of gradient in vapor concentration and low vapor diffusion coefficient, the impact of vapor diffusion on fluid movement is likely significantly less important than film flow and sediment wicking in this experimental system.

To close the book on the impact of vapor diffusion on the sustained infiltration into the coarse underlying layer, we also calculated vapor diffusion estimates based on DiCarlo's estimate (eq. 9 in DiCarlo et al. 1999) and based on a traditional Fickian approach applied to soils (Cass et al. 1984):

$$J_v = -a\alpha D\nabla\rho \qquad (15)$$

where J_v = the mass flux density of water vapor (kg m^{-2} s^{-1}),
D = the diffusion coefficient of water vapor in air (m^2 s^{-1}),
$\nabla\rho$ = the water vapor density gradient (kg m^{-4}),
a = the volumetric air-filled porosity (m^3 m^{-3}), and
α = a dimensionless tortuosity factor generally assumed to be 0.66 for isothermal flow.

The DiCarlo estimate is based on the conservative assumption that the unsaturated hydraulic conductivity contribution to the sum of liquid and vapor transport (eq. 2 in DiCarlo et al. 1999) is extremely small at very low fluid saturations, and also that the vapor condenses to liquid behind the vapor front even in the absence of a temperature gradient. The latter assumption is supported by many studies showing that vapor will condense, i.e., adsorb to porous materials, even though the porous material has the same temperature as the vapor. In Figure 15, the

DiCarlo and Fickian vapor diffusion estimates are compared to the measured infiltration rates for Experiment 1. The cumulative vertical flux in these figures was calculated based on the saturation measured at the front edge of the wetting front over time which was 10.8%, and takes into account the ambient relative humidity of 85%. The driving gradient for vapor transport is the relative difference between the saturated and ambient humitdiites. For a relative humidity of 85%, the actual measured vertical flux for the 8/20 angular sand experiment is approximately 10 times higher than the Fickian estimate and 3 times higher than the DiCarlo estimate. If the relative humidity was closer to 100% as one would expect for the closed box we used in these experiments, the DiCarlo and Fickian estimates would be even lower due to the lack of driving gradient, and it is therefore not possible to explain the observed infiltration into the 8/20 angular sand based on vapor diffusion-based phenomena.

To confirm our hypotheses and theoretically verify the proposed dominance of film flow in the capillary barrier experiment, we applied the equation for film flow infiltration based on Wenzel wetting developed by Hay et al. (2008):

$$x_{h-p} = \left[\frac{\gamma \delta^2}{4\mu} \left(\frac{(2\delta + \lambda)cos\theta - \lambda sin\theta}{\lambda \delta} \right) \right]^{1/2} t^{1/2} = St^{1/2} \quad (15)$$

Including a negative capillary pressure at the coarse/fine interface, the above equation becomes:

$$x_{h-p} = \left[\frac{\delta^2}{4\mu} \left(-P + \gamma \frac{(2\delta + \lambda)cos\theta - \lambda sin\theta}{\lambda\delta} \right) \right]^{1/2} t^{1/2} = St^{1/2} \qquad (15)$$

where $x_{h\text{-}p}$ = infiltration distance (cm),
γ = surface tension (7.2x 10^{-2} N/m for water at 20 °C),
δ = the average amplitude of surface features (nm),
λ = the average wavelength of surface features (nm),
μ = the kinematic viscosity (1.02 x 10^{-3} Pa-s at 20 °C),
t = time in seconds,
P = the capillary pressure at the coarse/fine interface (-3432 Pa),
S = sorptivity (or diffusion) term in $m/s^{1/2}$.

Using this relationship and the measured quantities obtained from atomic force microscopy measurements given in Table 6, we obtained a theoretical sorptivity term of 7.7 $cm/day^{1/2}$ for the 8/20 angular sand and 5.7 $cm/day^{1/2}$ for the 2/16 rounded sand using a contact angle of 7 degrees. Adjusting for tortuosity, the vertical length of travel is 1/3 the actual travel distance (Dullien 1992), the estimated diffusion terms become 2.3 $cm/day^{1/2}$ and 1.7 cm/day, which matches the 8/20 angular (tuff) and 2/16 rounded experimental values of 2.54 $cm/day^{1/2}$ and 1.42 $cm/day^{1/2}$ quite well, see Table 7 for summary.

It should be noted that the sorptivity term varies as a function of the contact angle of the sediment, Figure 16 below illustrates the relationship. Between a range of zero and fifteen the calculated sorptivity term fluctuates by approximately 0.2 $cm/day^{1/2}$.

3.8 Discussion

The phenomena observed during our study are likely due to the combined effect of the two processes, as water film infiltration and vapor diffusion rarely occur separate

from each other. In a similar experiment, Tidwell et al. (2003) proposed that because blue dye was absent in the infiltrated water (assuming that the large organic molecule would have been filtered out by films and evaporation) the observed slow, but constant, infiltration into the dry layer must be caused by the combined action of vapor diffusion and film flow. The initial rate of infiltration measured in the Tidwell et al. (2003) was 20 percent, slowing to 10 percent after 112 days. These rates are higher than the infiltration observed in these experiments, however that may be due to differences in experimental design.

The interaction of the two processes is schematically illustrated in Figure 16. Initially, water vapor flows through the sand and some of the vapor adsorbs on the grains (Figure 17a-b), while the rest flows or diffuses through the open space between grains (Tzevelekos et al. 2000). At increasing vapor pressures water continues to be adsorbed onto the grains in multiple layers as long as sufficient water vapor is provided by vapor diffusion for this process to take place (Figure 17b-c). Over time, sufficiently thick films may form to facilitate flow (Figure 17c-d). Eventually the films on adjacent grains can coalesce via capillary condensation, initially in the finer pores, resulting in enhanced permeability and actual capillary action (Figure 17e-f). However, the timescales over which we are observing water moving through the coarse material indicate that vapor diffusion is not the dominant mechanism. As indicated by Conca (1990), and our own supporting experiment, vapor adsorption is minimal even under conditions of near 100% relative humidity. Vapor diffusion and

capillary condensation onto similar crushed tuff material only accounted for a 2.4% change in intergranular moisture content. This is further supported by Jabro (2009), who found the rate of water vapor gain in larger soil aggregates to be minimal at room temperature.

In contrast, studies conducted by Bico and Quere and others (Bico et al. 2001; Bico et al. 2002; Quere 2002; Quere and Bico 2003; Ishino et al. 2004; Quere 2008) indicate that surface wetting resulting when water films flow over rough materials can occur nearly instantaneously. Martines et al. (2005) and Bico et al. (2001) illustrated that the movement of fluid across a surface of fabricated nanopatterns could be predicted by hemi-wicking theory, where fluid infiltration is a function of the wettability and surface geometry of a material. Using the Hay et al. (2008) expression relating sediment surface geometry to infiltration, we were able to estimate the sorptivity coefficient, which provided a reasonable approximation of infiltration into the underlying layer of the capillary barrier system in Experiment 1.

Differences in diversion capacity and barrier stability between Experiments 1 and 2 were likely due to the differences in surface properties of the 8/20 and 2/16 sands. As illustrated in Figure 4, and by the BET data, the surface of the 8/20 angular sand is significantly rougher than that of the 2/16 rounded sand. Experimental design and numerical modeling based on traditional hydrologic property measurements failed to predict the behavior of both capillary barrier systems. This is likely due to the

exclusion of surface properties and the lack of consideration of dry regime processes in the numerical model.

3.9 Conclusion

We conducted two capillary barrier experiments using almost identical initial and boundary conditions, but using different underlying (coarse) materials. The coarse materials had very similar hydrologic properties, but were morphologically different. The rounded sand (2/16) provided a better functioning capillary barrier than the angular sand (8/20), but neither of the materials (in combination with the fine Overton sand) provided a perfectly working capillary barrier. Our measurements of hydrologic parameters were typical of those routinely carried out for studies of unsaturated flow in porous materials. Our experimental results and data analyses indicated that prediction of capillary barrier performance based on standard hydrologic property parameter measurements is not always adequate for predicting detailed system behavior.

Our numerical simulations predicted that the barriers should be functioning perfectly for the measured material properties, with no infiltration into the coarse layer. When pseudo-optimized hydrologic parameters were used in the numerical model, we were able to simulate the barrier failure observed in the experiments, but not the observed differences between the two experiments. Thus, this exercise did not provide a mechanistic explanation of the actual differences in flow behavior. To explain the observed differences, we measured the surface profiles and roughness of the two

sands and conducted an additional vapor diffusion experiment. Based on theoretical calculations and vapor diffusion experiments, the primary controlling mechanism in this system appears to be the magnitude of surface area and roughness of the sediments, resulting in varying rates of infiltration due to differing film flow infiltration velocities.

Traditional numerical modeling and design, conducted using Richards' equation exclude dry regime flow processes, which can have significant impacts on flow and transport in dry systems in semi-arid and arid climates, and in particular at the Yucca Mountain, NV site. Therefore, for experiments conducted at low saturation, considering material characteristics (such as surface area and roughness) in addition to traditional hydrologic properties are necessary to fully describe the system behavior. We believe this is an especially important point to consider when dealing with capillary barrier design. Future numerical models could be improved by extending the hydraulic conductivity functions to mimic water film infiltration velocities as a function of surface roughness.

Despite the fact that water infiltrated the lower coarse material in both of our experiments, it is notable that the majority of the water was diverted by the drains in both cases (93.3% for the angular sand and 99.7% for the rounded sand). Depending on design requirements, this system may be considered a fully functioning capillary barrier. However, for more stringent design requirements, greater consideration of vapor diffusion and water film infiltration in material selection is required.

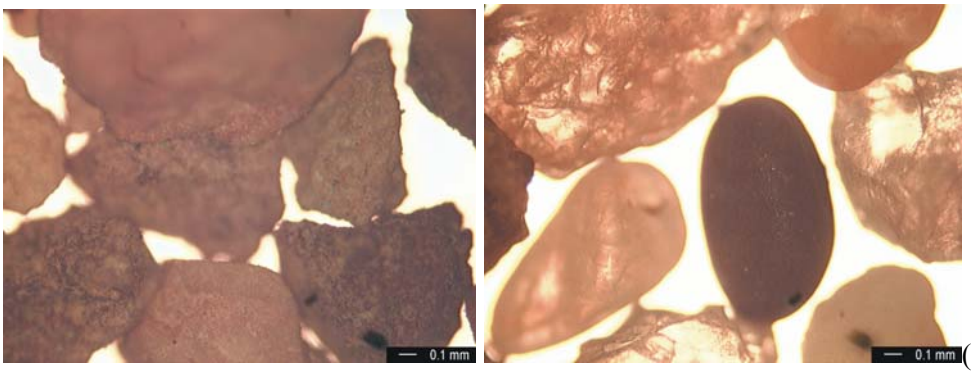

Figure 4. (Left) 8/20 angular sand (Right) 2/16 rounded sand

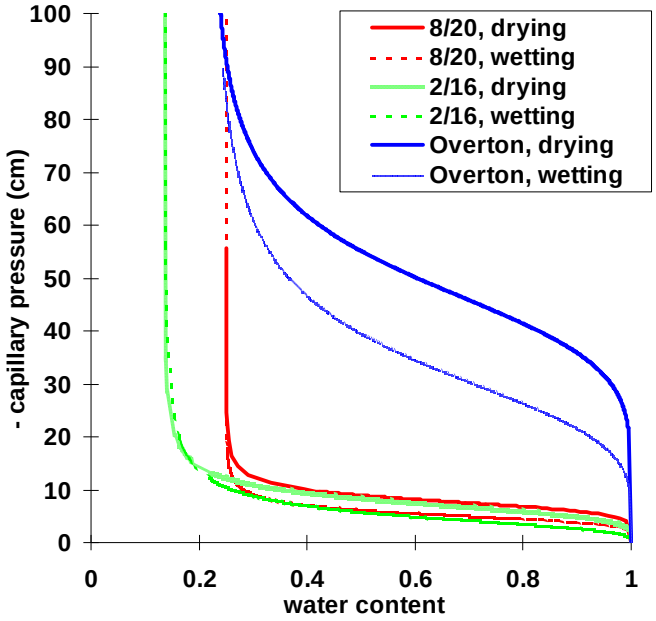

Figure 5. Pressure-saturation curve for 8/20, 2/16, and Overton sand

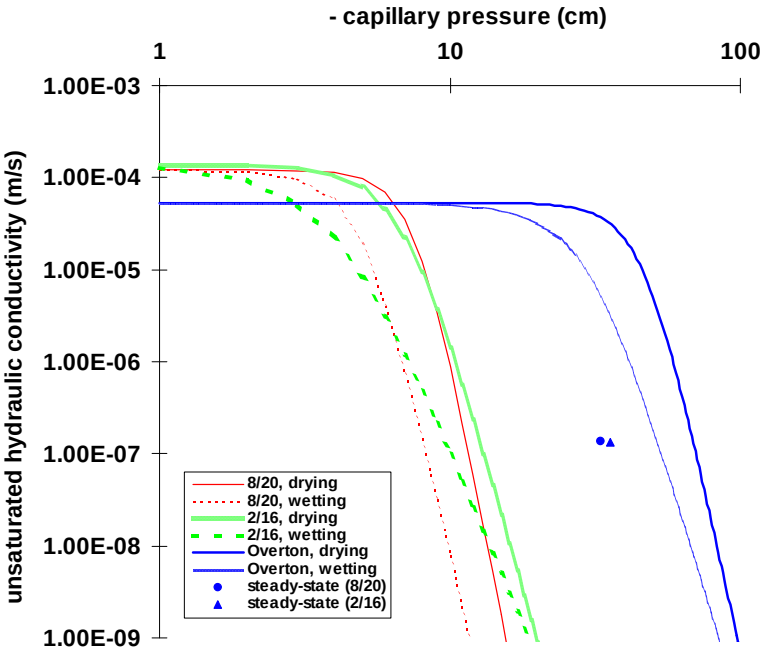

Figure 6. Pressure-conductivity curve for 8/20, 2/16, and Overton sand.Points indicate K_{unsat} during drainage

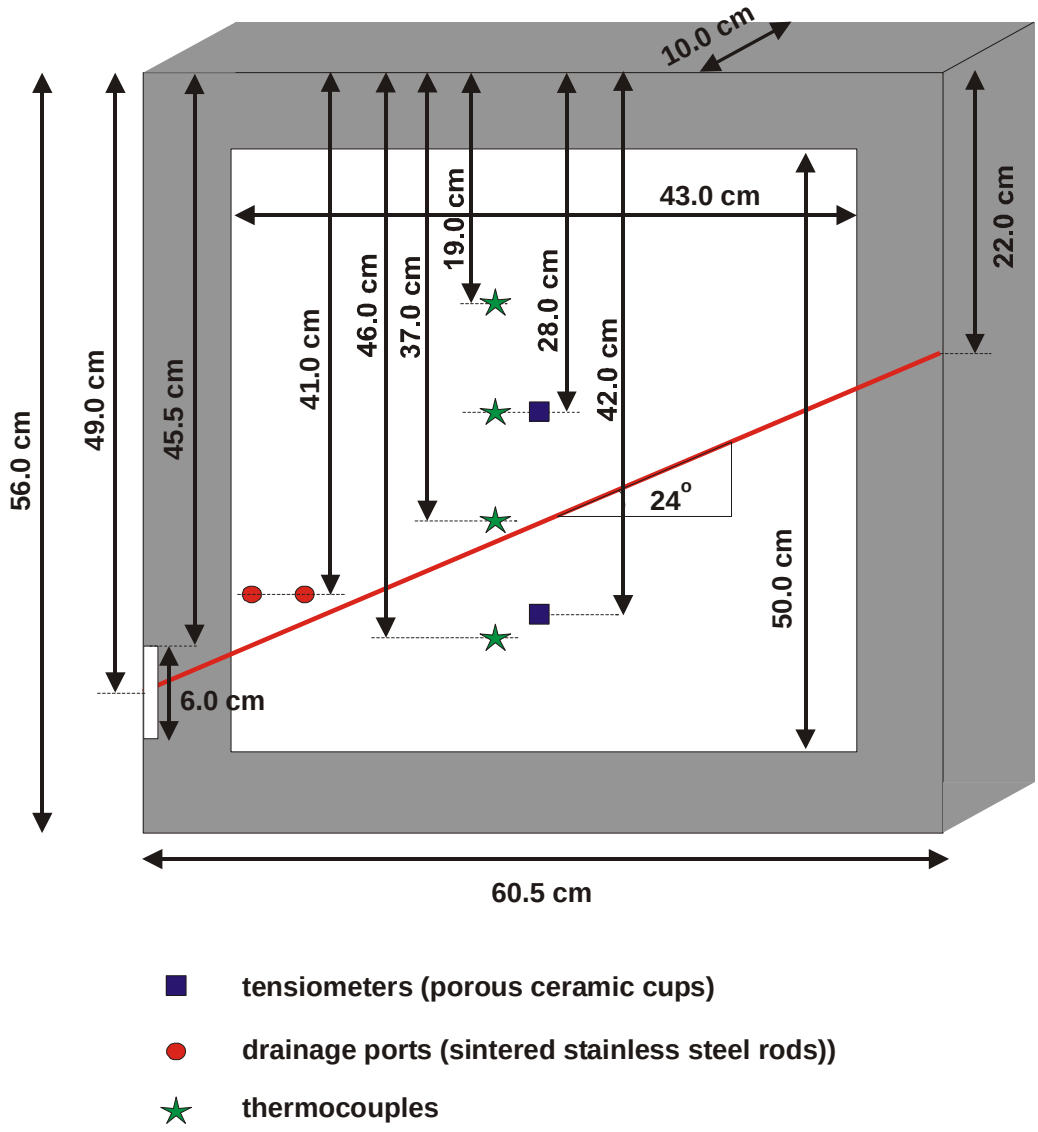

Figure 7. Experimental setup

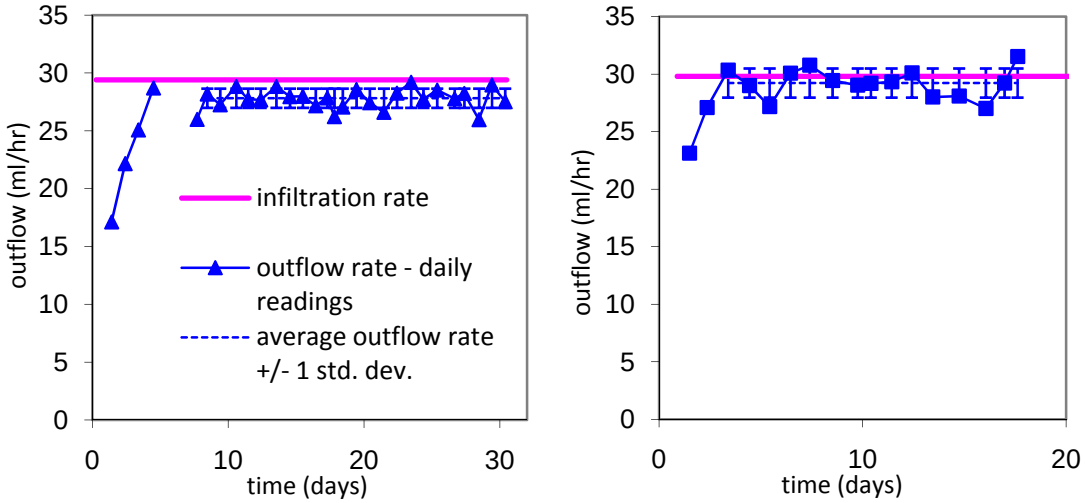

Figure 8. (Left) Water balance for Experiment 1 (Overton over 8/20 angular sand), (Right) Water balance for Experiment 2 (Overton sand over 2/16 rounded sand).

Figure 9. (Top) Dye tracer transport time-lapse for Experiment 1 (8/20 sand), (Bottom) Dye tracer transport time-lapse for Experiment 2 (2/16 sand)

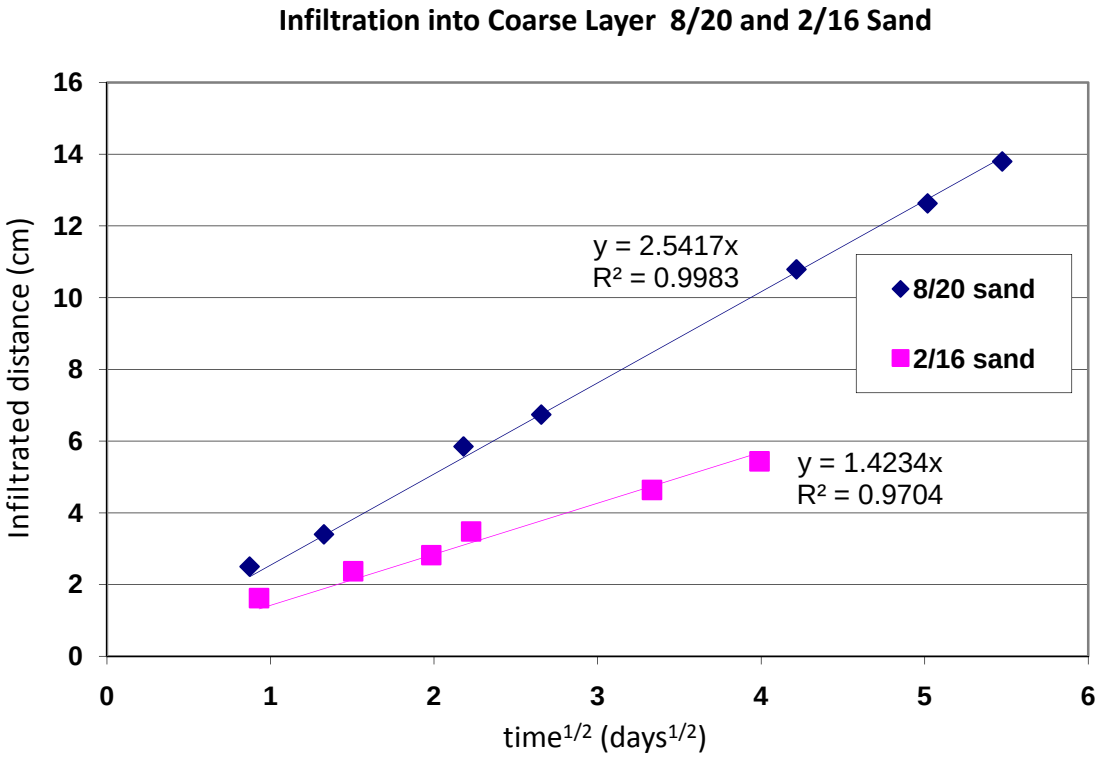

Figure 10. Infiltration distance versus the square root of time in Experiment 1 (pink) and Experiment 2 (blue)

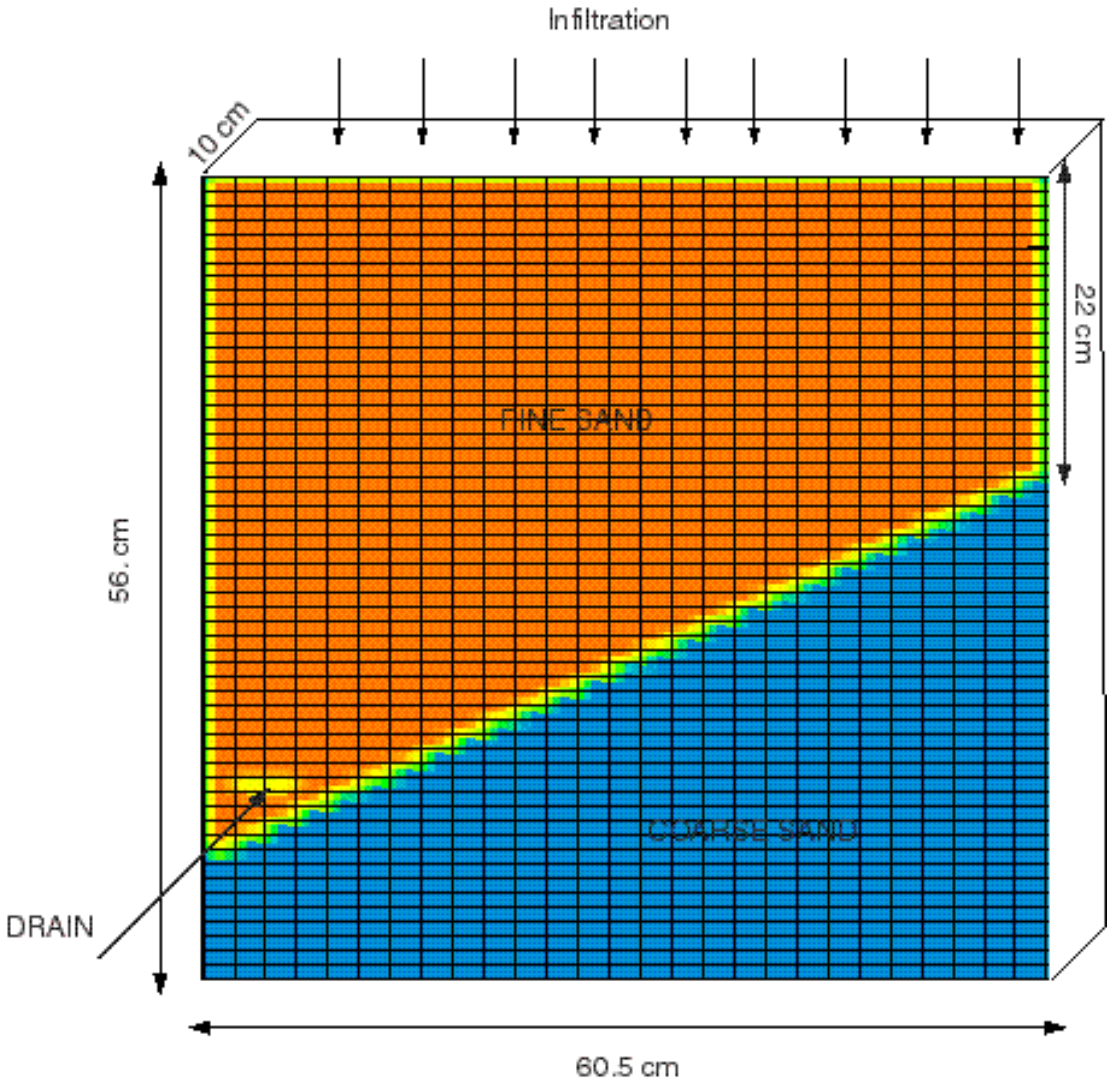

Figure 11. Experimental domain for the NUFT modeling of capillary barrier system.

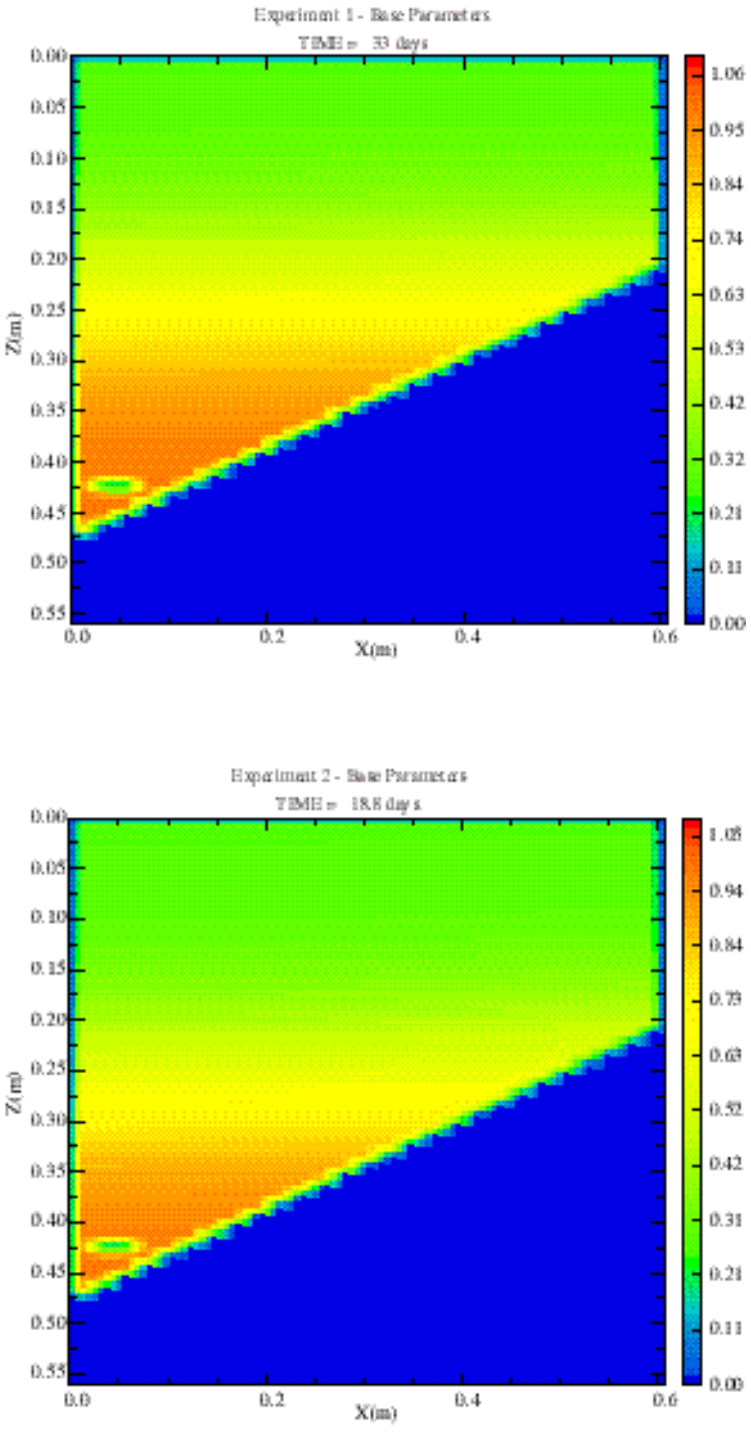

Figure 12. Simulated saturation fields for Experiments 1 (Top) and 2 (Bottom) using the base parameters given in Table 4.

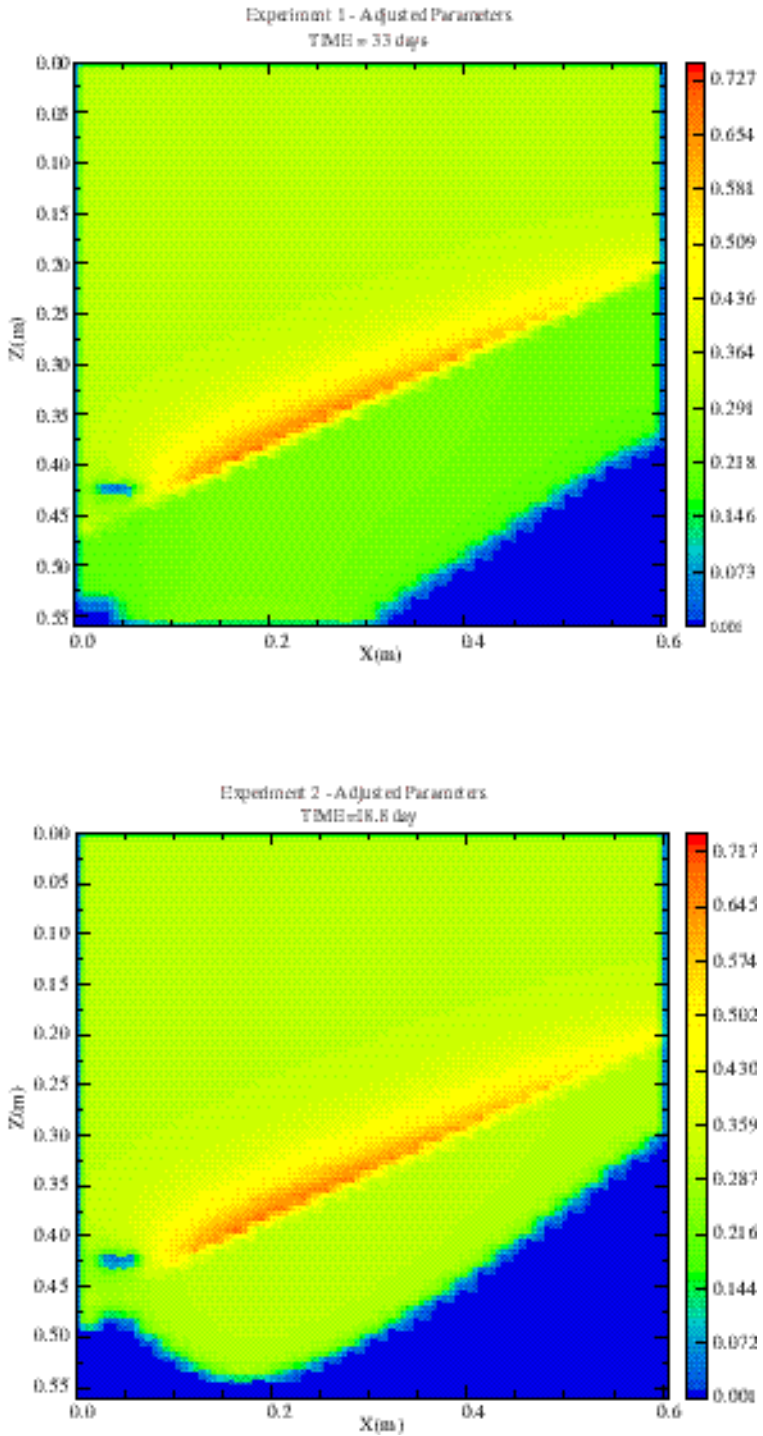

Figure 13. Simulated saturation fields for Experiments 1 and 2 using the adjusted parameters given in Table 5.

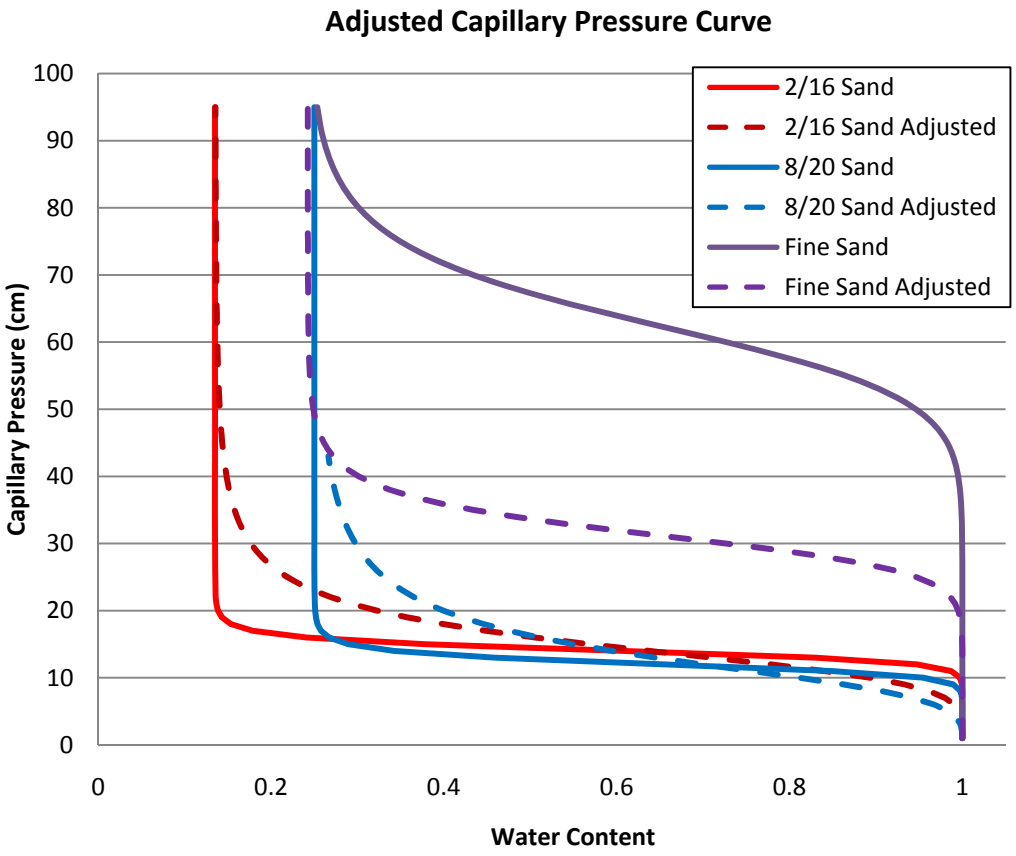

Figure 14. Capillary pressure saturation curve for adjusted NUFT input parameters

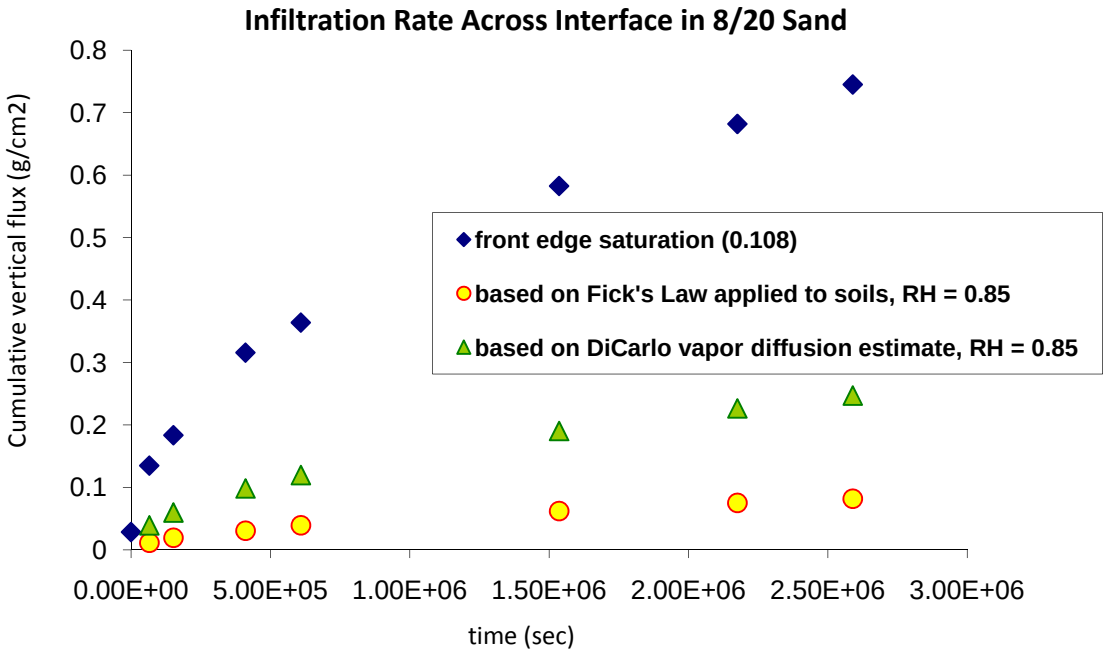

Figure 15. Vapor diffusion into crushed tuff using Fick's Law and DiCarlo estimate calculated using the measured saturation at the front of the wetting front

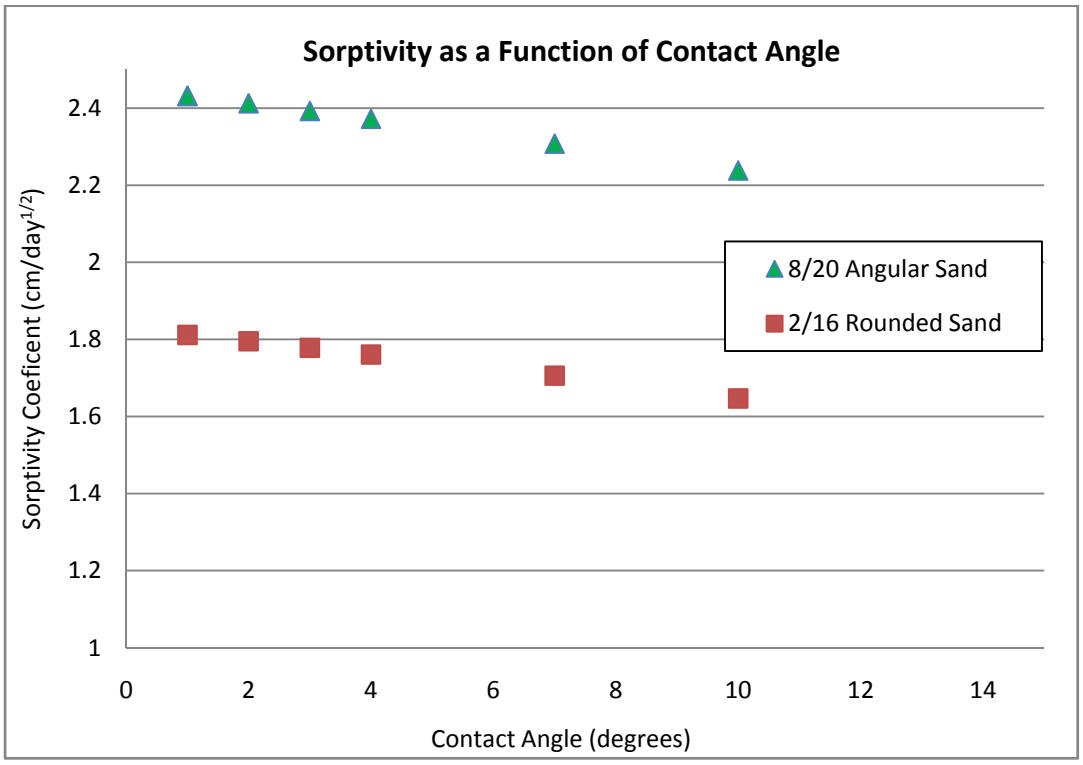

Figure 16. Sorptivity of infiltrating film as a function of contact angle

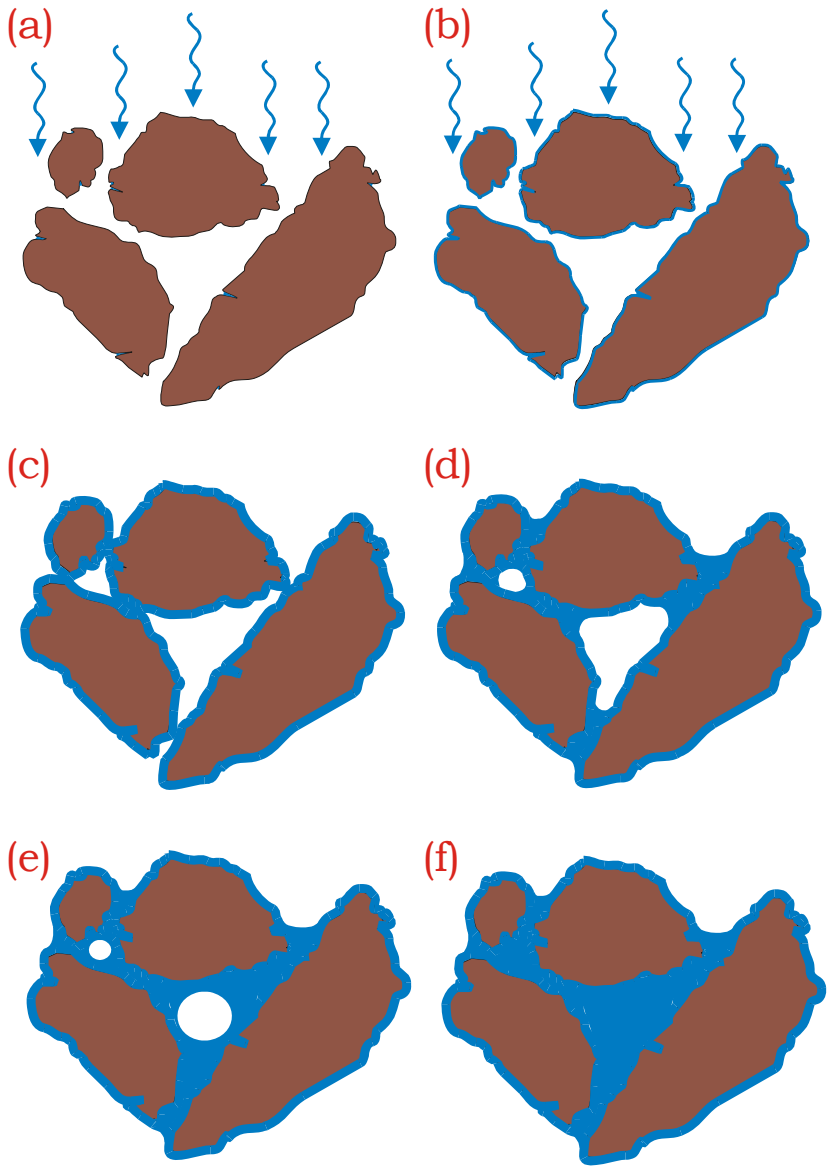

Figure 17. Hypothesized combined effect of vapor diffusion and film flow on the initial infiltration into dry soils.

Table 1. Material properties

grain size distribution (mm)	8/20 angular	2/16 smooth	Overton fine
0.053	0.47	-	2.08
0.1	0.77	-	55.58
0.25	1.27	0.06	39.24
0.42	-	0.54	-
0.5	32.7	-	3.06
0.575	-	2.23	-
1.0	64.83	62.73	0
1.41	-	34.19	-
2.0	2	0.21	0
d^{50}	0.58	0.87	0.091
d^{60}/d^{10}	3.42	1.56	2.07
surface area (m^2/g)			
Total	2.908	0.227	
micropore	0.230	0.040	

Table 2. Material hydrologic properties

	α (cm^{-1})	n	θs	θr	R^2	K_s (m/s)
2/16 drying	0.139	4.69	0.37	0.05	0.997	
2/16 wetting	0.231	3.25	0.37	0.05	0.997	$1.4\ 10^{-4}$
8/20 drying	0.130	6.65	0.48	0.12	0.996	
8/20 wetting	0.197	5.64	0.48	0.12	0.998	$1.2\ 10^{-4}$
Overton drying	0.021	6.06	0.37	0.08	0.999	
Overton wetting	0.032	4.39	0.37	0.08	0.999	$5.3\ 10^{-5}$

Table 3. Flow rates and boundary conditions for the experiments.

	Experiment 1 Overton over 8/20	Experiment 2 Overton over 2/16
average pump rate (ml/h)	29.8	29.3
average pump rate (m/s)	$1.37\ 10^{-7}$	$1.35\ 10^{-7}$
average outflow rate (ml/h)	27.8 +/- 0.8	29.2 +/- 1.3
average fine layer suction (cm)	32.9 +/- 2.8	35.7 +/- 2.8
average drain suction (cm)	43.2 +/-1.5	46.3 +/- 2.1

Table 4. NUFT base input parameters

	Experiment 1 Fine = Overton Coarse = 8/20 angular	Experiment 2 Fine = Overton Coarse = 2/16 rounded
Infiltration rate (m/s)	1.37e-7	1.35e-7
Drain suction (m)	0.432	0.463
Fine sand:		
K_s (m/s)	5.3e-5	5.3e-5
α (m^{-1})	1.6	1.6
M	0.91	0.91
S_r	0.18	0.18
ϕ	0.33	0.33
Coarse sand:		
K_s (m/s)	1.2e-4	1.4e-4
α (m^{-1})	8.3	7.1
M	0.93	0.94
S_r	0.28	0.18
ϕ	0.48	0.37

Table 5. Summary of adjusted NUFT input parameters for model fit.

	Experiment 1 Fine = Overton Coarse = 8/20 angular		Experiment 2 Fine = Overton Coarse = 2/16 rounded	
	Table 5 values	adjusted values	Table 5 values	adjusted values
Fine sand:				
K_s (m/s)	5.3e-5	2e-5	5.3e-5	2e-5
α (m^{-1})	1.6	3.2	1.6	3.2
Coarse sand:				
K_s (m/s)	1.2e-4	6.e-5	1.4e-4	1.e-4
m	0.93	0.75	0.94	0.8

Table 6. Summary of measured sediment surface characteristics

	8/20 angular sand	2/16 rounded sand
Amplitude (δ)	3.8 nm	2.5 nm
Wavelength (λ)	50.0 nm	2000.0 nm

Chapter 4: Bibliography

Atkins, P., and J. De Paula. 2006. Atkins' physical chemistry. 8th ed. Freeman and Company, New York.

Bear, J. 1972. Dynamics of fluids in porous media. Elsevier, New York.

Bear, J. 1988. Dynamics of fluids in porous media. Dover Publications, New York.

Bico, J., U. Thiele, et al. 2002. Wetting of textured surfaces. Colloids and Surfaces a-Physicochemical and Engineering Aspects 206:41-46.

Bico, J., C. Tordeux, et al. 2001. Rough wetting. Europhysics Letters 55:214-220.

Brooks, R.H., and A.T. Corey. 1964. Hydraulic properties of porous media. Colorado State University, Fort Collins, CO.

Brunauer, S., P.H. Emmett, et al. 1938. Adsorption of gases in multimolecular layers. Journal of the American Chemical Society 60:309-319.

Carter, L.J., and T.H. Pigford. 2005. Nuclear waste - proof of safety at yucca mountain. Science 310:447-448.

Cass, A., G.S. Campbell, et al. 1984. Enhancment of thermal water vapor diffusion in soil. Soil Science of America 48:25-32.

Cassie, A.B.D., and S. Baxter. 1944. Wettability of porous surfaces. Transactions of the Faraday Society 40:0546-0550.

Christenson, H.K. 1994. Capillary condensation due to van-der-waals attraction in wet slits. Physical Review Letters 73:1821-1824.

Churaev, N.V. 2003. Derjaguin's disjoining pressure in the colloid science and surface phenomena. Advances in Colloid and Interface Science 104:Xv-Xx.

Conca, J.L. 1990. Diffusion barrier transport properties of unsaturated paintbrush tuff rubble backfill. . Proceedings of the First International High-Level Radioactive Waste Managment Conference, Las Vegas, NV.:p. 394-401.

Conca, J.L. 1998. Flow barrier system for long-term high-level-waste isolation: Experimental results. Nuclear Technology 124:88-100.

Conca, J.L. 1999. Flow barrier system for long-term high-level-waste isolation: Experimental results - reply. Nuclear Technology 126:241-241.

Conca, J.L., and J. Wright. 1990. Diffusion-coefficients in gravel under unsaturated conditions. Water Resources Research 26:1055-1066.

Corey, A.T., and S.D. Logsdon. 2005. Limitations of the chemical potential. Soil Science Society of America Journal 69:976-982.

Culligan, P.J., V. Ivanov, et al. 2005. Sorptivity and liquid infiltration into dry soil. Advances in Water Resources 28:1010-1020.

Derjaguin, B.V., and N.V. Churaf. 1974. Polymolecular adsorption and capillary condensation in narrow slit pores. Journal of Colloid and Interface Science 54:157-174.

DiCarlo, D.A., T.W.J. Bauters, et al. 1999. Lateral expansion of preferential flow paths in sands. Water Resources Research 35:427-434.

Dullien, F. 1992. Porous media:Fluid transport and pore structure. Academic Press, Waterloo, Ontario, Canada.
Easton, E.B., and W.D. Machin. 2000. Adsorption of water vapor on a graphitized carbon black. Journal of Colloid and Interface Science 231:204-206.
Green, W.H., and G.A. Ampt. 1911. Studies on soil physics part i - the flow of air and water through soils. Journal of Agricultural Science 4:1-24.
Hay, K.M., M.I. Dragila, et al. 2008. Theoretical model for the wetting of a rough surface. Journal of Colloid and Interface Science 325:472-477.
Hillel, D. 1998. Environmental soil physics. Academic Press, San Diego.
Hsieh, D.Y., and X.P. Wang. 1997. Phase transition in van der waals fluid. Siam Journal on Applied Mathematics 57:871-892.
Hu, Q., T. Kneafsey, et al. 2004. Characterizing unsaturated diffusion in porous tuff gravel. Vadose Zone Journal 3:1425-1438.
Ishino, C., K. Okumura, et al. 2004. Wetting transitions on rough surfaces. Europhysics Letters 68:419-425.
Iwamatsu, M., and K. Horii. 1996. Capillary condensation and adhesion of two wetter surfaces. Journal of Colloid and Interface Science 182:400-406.
Jabro, J.D. 2009. Water vapor diffusion through soil as affected by temperature and aggregate size. Transport in Porous Media 77:417-428.
Jones, S.B., and D. Or. 2002. Surface area, geometrical and configurational effects on permittivity of porous media. Journal of Non-Crystalline Solids 305:247-254.
Kampf, M., T. Holfelder, et al. 2003. Identification and parameterization of flow processes in artificial capillary barriers. Water Resources Research 39:-.
Klute, A. 1986. Methods of soil analysis, part 1. 2nd ed. ASA and SSA, Madison, WI.
Kutilek, M., and D.R. Nielsen. 1994. Soil hydrology. [Online], Catena-Verlag, Germany.
Liu, H.H. 2004. A constitutive-relationship model for film flow on rough fracture surfaces. Hydrogeology Journal 12:237-240.
Martines, E., K. Seunarine, et al. 2005. Superhydrophobicity and superhydrophilicity of regular nanopatterns. Nano Letters 5:2097-2103.
Miller, E.E., and R.D. Miller. 1956. Physical theory for capillary flow phenomena. Journal of Applied Physics 27:324-332.
Mualem, Y. 1976. Hysteretical models for prediction of hydraulic conductivity of unsaturated porous-media. Water Resources Research 12:1248-1254.
Muller, H.J. 1998. Extraordinarily thick water films on hydrophilic solids: A result of hydrophobic repulsion? Langmuir 14:6789-6792.
Nimmo, J.R., D.A. Stonestrom, et al. 1994. The feasibility of recharge rate determinations using the steady-state centrifuge method. Soil Science Society of America Journal 58:49-56.
Nitao, J.J. 1998. Referebce manual for the nuft flow and transport code version 2.0. Lawrence Livermore National Laboratory.

Nitao, J.J., and J. Bear. 1996. Potentials and their rold in transport in porous media. Water Resources Research 32:225-250.
Nitao, J.J., and T.A. Buscheck. 1991. Infiltration of a liquid front in an unsaturated, fractured porous-medium. Water Resources Research 27:2099-2112.
Oldenburg, C.M., and K. Pruess. 1993. On numerical modeling of capillary barriers. Water Resources Research 29:1045-1056.
Or, D., and M. Tuller. 1999. Liquid retention and interfacial area in variably saturated porous media: Upscaling from single-pore to sample-scale model. Water Resources Research 35:3591-3605.
Or, D., and M. Tuller. 2000. Flow in unsaturated fractured porous media: Hydraulic conductivity of rough surfaces. Water Resources Research 36:1165-1177.
Parker, J. 1986. Hydrostatics of water in porous media. [Online] CRC Press, Boca Raton, Fl.
Philip, J.R. 1977. Unitary approach to capillary condensation and adsorption. Journal of Chemical Physics 66:5069-5075.
Pismen, L.M. 2001. Nonlocal diffuse interface theory of thin films and the moving contact line. Physical Review E 6402:-.
Porro, I. 2001. Hydrologic behavior of two engineered barriers following extreme wetting. Journal of Environmental Quality 30:655-667.
Quere, D. 2002. Rough ideas on wetting. Physica a-Statistical Mechanics and Its Applications 313:32-46.
Quere, D. 2008. Wetting and roughness. Annual Review of Materials Research 38:71-99.
Quere, D., and J. Bico. 2003. Controlled wetting by surface patterning. Houille Blanche-Revue Internationale De L Eau:21-24.
Ross, B. 1990. The diversion capacity of capillary barriers. Water Resources Research 26:2625-2629.
Smesrud, J.K., and J.S. Selker. 2001. Effect of soil-particle size contrast on capillary barrier performance. Journal of Geotechnical and Geoenvironmental Engineering 127:885-888.
Steenhuis, T.S., J.Y. Parlange, et al. 1991. The diversion capacity of capillary barriers - comment. Water Resources Research 27:2155-2156.
Tidwell, V.C., R.J. Glass, et al. 2003. Visualization experiment to investigate capillary barrier performance in the context of a yucca mountain emplacement drift. Journal of Contaminant Hydrology 62-3:287-301.
Tokunaga, T.K. 1997. A tensiometer for measuring hydraulic potentials on surfaces of porous rock. Water Resources Research 33:1509-1513.
Tokunaga, T.K. 2009. Hydraulic properties of adsorbed water films in unsaturated porous media. Water Resources Research 45:-.
Tokunaga, T.K., and J.M. Wan. 1997. Water film flow along fracture surfaces of porous rock. Water Resources Research 33:1287-1295.

Tokunaga, T.K., and J.M. Wan. 2001. Approximate boundaries between different flow regimes in fractured rocks. Water Resources Research 37:2103-2111.

Tokunaga, T.K., and J.M. Wan. 2001. Surface-zone flow along unsaturated rock fractures. Water Resources Research 37:287-296.

Tokunaga, T.K., J.M. Wan, et al. 2000. Transient film flow on rough fracture surfaces. Water Resources Research 36:1737-1746.

Tuller, M., and D. Or. 2001. Hydraulic conductivity of variably saturated porous media: Film and corner flow in angular pore space. Water Resources Research 37:1257-1276.

Tuller, M., and D. Or. 2005. Water films and scaling of soil characteristic curves at low water contents. Water Resources Research 41:-.

Tuller, M., D. Or, et al. 1999. Adsorption and capillary condensation in porous media: Liquid retention and interfacial configurations in angular pores. Water Resources Research 35:1949-1964.

Tzevelekos, K.P., E.S. Kikkinides, et al. 2000. Adsorption-desorption flow of condensable vapors through mesoporous media: Network modeling and percolation theory. Journal of Colloid and Interface Science 223:89-101.

van Genuchten, M. 1980. A closed form equation for predicting the hydraulic conductivity of unsaturated soils. Soil Science Society of America Journal 49:1354-1359.

Webb, S., and C.K. Ho. 1998. Enhanced vapor-phase diffusion in porous media, ldrd final report. Sandia National Laboratories, Albuquerque, New Mexico.

Webb, S.W. 1997. Generalization of ross' tilted capillary barrier diversion formula for different two-phase characteristic curves. Water Resources Research 33:1855-1859.

Weeks, S.W., G.C. Sander, et al. 2004. Saturated and unsaturated water flow in inclined porous media. Environmental Modeling & Assessment 9:91-102.

Wenzel, R.N. 1936. Resistance of solid surfaces to wetting by water. Industrial and Engineering Chemistry 28:988-994.

Wildenschild, D., K.H. Jensen, et al. 1997. A two-stage procedure for determining unsaturated hydraulic characteristics using a syringe pump and outflow observations. Soil Science Society of America Journal 61:347-359.

Wildenschild, D., and J.J. Roberts. 2001. Experimental tests of enhancement of vapor diffusion in topopah spring tuff. Journal of Porous Media 4:1-13.

Wu, Y.S., W. Zhang, et al. 2002. Modeling capillary barrier in unsaturated fractured rock. Water Resources Research 38.

Yanful, E.K., S.M. Mousavi, et al. 2006. A numerical study of soil cover performance. Journal of Environmental Management 81:72-92.

Zhang, Q., A.D. Werner, et al. 2009. Influence of soil moisture hysteresis on the functioning of capillary barriers. Hydrological Processes 23:1369-1375.